PL ISSN 0209–0066

INSTYTUT
TECHNOLOGII
MATERIAŁÓW
ELEKTRONICZNYCH

PRACE
ITME

ANDRZEJ L. BAJOR

SOME PROBLEMS OF OPTICAL INHOMOGENEITY TESTING IN CRYSTALLINE MATERIALS BY IMAGING POLARIMETRY

1996

Zeszyt 47

INSTYTUT TECHNOLOGII MATERIAŁÓW ELEKTRONICZNYCH

Andrzej L. Bajor

SOME PROBLEMS OF OPTICAL INHOMOGENEITY TESTING IN CRYSTALLINE MATERIALS BY IMAGING POLARIMETRY

WARSZAWA ITME 1996

Adres Redakcji:

INSTYTUT TECHNOLOGII MATERIAŁÓW ELEKTRONICZNYCH
ul. Wólczyńska 133, 01-919 Warszawa, email: itme4@atos.warman.com.pl

tel.	35 44 16 lub 35 30 41 w. 454	- redaktor naczelny
	35 30 41 w. 164	- z-ca redaktora naczelnego
	35 30 41 w. 129	- sekretarz redakcji

PL ISSN 0209 - 0066

Skład i grafika komputerowa - ITME
Andrzej Karwize (karwiz_a@sp.itme.edu.pl)

Andrzej Leopold Bajor was born in Warsaw in 1952. In 1974 he has acquired M.Sc. degree in electronic engineering from the Warsaw University of Technology. In the years 1974-1979 he was employed by the Institute of Electron Technology (Warsaw). Since 1979 he has been employed by the Institute of Electronic Materials Technology (Warsaw), currently as a senior researcher. His main activities in the ITME are optical testing of semiconducting and oxide crystals and development of testing equipment. He is an author or co-author of 31 papers in technical and scientific journals and 11 (Polish) patents, two grants acquired from the Polish Committee for Scientific Research (computerized imaging polarimeter, and computerized imaging conoscope). Member of SPIE and of the Polish Society for Crystal Growth.

SOME PROBLEMS OF OPTICAL INHOMOGENEITY TESTING IN CRYSTALLINE MATERIALS BY IMAGING POLARIMETRY

Received: 1995.12.04
Accepted for publication: 1996.02.20

In this work some problems associated with optical inhomogeneity testing in crystalline materials, including sources of optical inhomogeneity and its influence on materials' performance, advantages and disadvantages of different testing methods with particular attention payed to imaging polarimetry, are presented. A brief description is provided on principles of operation and working abilities of the computer-controlled imaging polarimeter developed in the ITME. It is capable of measuring plane-parallel samples with diameters up to 150 mm, and up to 10 mm thick, in the wavelength range of 0.4 - 1.15 μm. The basic sensitivities/accuracies of the device are : birefringence $\leq 5 \times 10^{-7}$, principal azimuth (one of the principal residual stress directions) < 1°, and transmission < 1 %. Several examples of measurements carried out on semiconducting and oxide crystals produced in the ITME, like GaAs and $LiNbO_3$, respectively, have been shown.

1. INTRODUCTION

Optical inhomogeneity is one of the most important parameters of crystalline materials widely used in optics and electronics. In this monograph after a brief introduction to the problem of optical inhomogeneity and its testing presented in chapter 2, the subsequent chapters are devoted to the construction and use of an automated, computer-controlled imaging polarimeter developed in the ITME.

The polarimeter comprising only two large sheet linear polarizers as the modulating elements, is capable for real-time birefringence/stress and transmission mapping in large-area wafers or slabs (up to 6 inches in diameter and up to 0.4 inch thick, respectively) cut out from the investigated materials. By using a modified Carré method it is possible to acquire in a single measurement step all necessary data for calculating three maps: birefringence (natural or stress induced), the principal azimuth of the retarder (one of the principal residual stress directions) and transmission. By applying the piezo-elasto-optical coefficients of the material published elsewhere it is also possible to calculate and plot the residual stress map besides the usually acquired birefringence map.

After a brief description of principles of the method given in chapter 3, only a short information on polarimeters's construction (chapter 4) is provided, since it had been described in details in earlier works [1,2]. However, an emphasis is made upon mapping procedures presented in chapters 3.1 and 3.2, having a strict connection with optimization of sensitivity of the measurements (chapter 5). Although the polarimeter can be used for investigation of all kinds of materials (e.g. polycrystals and glasses) transparent in the absorption range of a silicon CCD matrix (0.4 to 1.15 μm) used in camera system, chapter 6 is merely devoted to birefringence or stress inhomogeneity testing in semiconducting and oxide crystals, being the two main fields of ITME's activity in materials production. The other important reason is that residual birefringence/stress testing in such crystals is a powerful tool for optimization of their technologies, and especially of the most widely used Czochralski growth method.

2. SOME PROBLEMS ASSOCIATED WITH OPTICAL INHOMOGENEITY TESTING IN TRANSPARENT MATERIALS

2.1 DEFINITIONS

Optical inhomogeneity (**OI**) is described as the refractive index or birefringence change per unit length L of the material, i.e.

$$B = \frac{\delta n}{\delta L} \tag{1}$$

or

$$B = \frac{\delta(\Delta n)}{\delta L} = \frac{\delta(n_e - n_o)}{\delta L} \tag{2}$$

where B is optical inhomogeneity in units of cm^{-1}, n is refractive index, and n_e and n_o are the extraordinary and ordinary refractive indices, respectively.

Birefringence Δn, i.e. the difference of extraordinary and ordinary refractive indices is either positive or negative for the so called positive or negative uniaxial crystals, respectively. Birefringence can be calculated either from retardation data normally acquired in any of numerous polarimetric configurations using a well known formula

$$\Delta n = \frac{\lambda \delta}{2\pi d} \tag{3}$$

where λ is wavelength, δ is (phase) retardation, and d is sample thickness, or by

measuring separately the two refractive indices n_e and n_o, usually by the prism minimum deviation method in a goniometer.

A polarimeter, also called a transmission ellipsometer, and sometimes (improperly) - a polariscope, can be either a very simple or a sophisticated measuring equipment. In its simplest configuration of a linear polarimeter it comprises a light source, a condensor system for producing a parallel beam of light, a pair of linear polarizers, a detector of electromagnetic radiation placed after the second polarizer (the analyzer) and a sample's holder placed between the two polarizers. An analysis carried out by the author [1] has indicated that this simplest polarimetric configuration is capable for acquiring all necessary data for calculating all three above mentioned maps. Hence, no other commonly used polarimetric configurations comprising e.g. retardation (quarterwave) plates or photoelastic modulators has been further considered, since for obvious reasons any additional optical element in the light path is an unavoidable source of additional errors [3-5]. Thus in further considerations a term **polarimeter** means a **linear polarimeter**, and also the term polarimetric configuration refers to its simplest version.

The last thing that has to be defined here is an optical indicatrix or the (refractive) index ellipsoid. Its equation as defined in general case for biaxial crystal in e.g. [6,7] is given by

$$\frac{x^2}{n_1^2} + \frac{y^2}{n_2^2} + \frac{z^2}{n_3^2} = 1 \tag{4}$$

where x,y, and z, are the principal axes of the ellipsoid, and n_1, n_2, and n_3 are the respective principal refractive indices. The $1/n_i^2$ terms in eq. (4) (frequently denoted by B_i) are the components of the so called dielectric impermeability tensor [B] very often used in optical calculations [6].

In an isotropic material $n_1=n_2=n_3=n_o$ and eq. (4) represents a sphere, i.e. the refractive index is independent on the direction of the light ray in the material.

In an uniaxial crystal (or precisely speaking - uniaxial material) $n_1=n_2=n_o$ and $n_3=n_e$, and the ellipsoid has only one cross section of constant index of refraction equal to n_o. A direction (a principal axis) perpendicular to this cross section is called an optical axis of a uniaxial crystal, and it is the only direction for which no relative retardation occurs between the ordinary and extraordinary rays. A plane-polarized light beam travelling along this direction does not see any anisotropic properties on its way, and so the crystal behaves like an isotropic material for the direction of its optical axis. This is an important property since many crystals owe large natural birefringences and the only practical possibility for investigating the optical inhomogeneity involved by other (than inherent) effects, like e.g. residual stresses, is to cut out a sample perpendicularly to its optical axis.

2.2 SOURCES OF OPTICAL INHOMOGENEITY

There are several sources of optical inhomogeneity of a crystal (material) and these can be briefly described as follows:

1/ **Nonstoichiometry.** It is a well known fact, for example, that the natural birefringence in $LiNbO_3$ undoped crystals is highly dependent on [Li]/[Nb] ratio [8,9]. Since this birefringence is very large ($8\text{-}9\times10^{-2}$), even small variations of stoichiometry will involve relatively large birefringence changes in crystal's volume, larger than those expected from residual stresses ($10^{-6}\text{-}10^{-5}$). Thus it is clearly evident that in $LiNbO_3$ crystals, and also in crystals owing much smaller birefringences like e.g. $LiTaO_3$ (5×10^{-3}) it is practically impossible to distinguish for other directions than the optical axis itself whether the **OI** changes are due to stoichiometric variations or to some other effects.

2/ **Doping.** An obvious fact that doping a host material with alien ions should lead to a change in refractive index is one of the primary reasons and sources for the **OI** effect. The effect of doping can, however, influence the **OI** in two ways.

Due to differences in size between the host ions and the dopants a certain birefringence will always occur through the piezooptical effect (deformation of the crystal's lattice). If the doping concentration is low, however, this birefringence can be of an insignificant value. Nevertheless, the influence of dopant on the refractive index still remains. If the dopant is uniformly distributed in crystal's (material's) volume than no **OI** effect exists. If not, a certain **OI** due to the refractive index change per unit length (eq. (1)) appears.

There might be, however, one exception in this last case. Imagine for example a point diffusion source and the doping diffusion profiles to be spherical in shape. If a point light source emits radiation along the radii of the sphere then neither birefringence-like effects nor any curvature of the light rays occur. Thus we can talk about a quasihomogeneity of the crystal for the directions of the diffusion paths in spite of the refractive index changes along these directions. In general case, however, and also for every other direction differing from the diffusion paths, a general formula (1) describes the **OI** effect induced by even small changes of the refractive index.

The doping concentrations in nowadays crystalline materials may, however, be very large as e.g. in $Y_3Al_5O_{12}$ (YAG) crystals doped heavily with Er^{3+} ions for coherent light generation. The doping concentrations in this example can be as high as 30-50 % [10], i.e. approximately every second yttrium ion is replaced by the erbium ion. It is clear that such large erbium ions content should have a considerable influence on lattice deformation, and hence, on the **OI** through the piezooptical effect. So in the case of doping we have to deal with two effects influencing the **OI**, i.e. the effects associated with lattice deformation and refractive index changes due to coloration.

3/ **Residual stresses.** It is estimated that almost 1/3 of the maximum resolved shear stress generated by thermal gradients during Czochralski-growth remains un-

dissipated after the pulled crystal had been cooled down [11]. Residual stresses through the piezooptical effect involve birefringence changes in crystal's volume. Depending on the material under manufacture (isotropic (glass) or anisotropic (elemental or compound crystal)), the growth conditions and orientation of the crystal, the residual stresses in practical circumstances can be insignificantly low and through 10^5 - 10^7 Pa (moderate values) they can reach 10^8 - 10^9 Pa in highly stressed crystals. Providing that the so called piezooptical constant of the material is of the order of 10^{-13} Pa^{-1}, the adequate birefringence changes involved by the largest residual stresses would be approximately equal to 10^{-5} - 10^{-4}. It will be said later that such birefringence changes in the material are nonadmissible in almost all of its optical applications.

4/ **Structural imperfections.** Although a major fraction of thermal stresses generated by thermal gradients during material's manufacture is dissipated in the cooling process or frozen in the material as the frozen in (residual) stresses, it may happen that a portion of it is involved in creating defects like dislocations and even microcracks. Generally speaking, any defect like a dislocation, a void or inclusion, is surrounded by a local deformation of the lattice, and hence, by a local stress field. It may happen that the local stress fields yield zero along a larger distance due to changes in sign of the stresses, but locally they always generate birefringence changes due to the piezooptical effect. Depending on the locality and diameter of the light beam passing through the material these changes can exclude it from most potential optical applications.

5/ **Optical anisotropy.** The inherent anisotropic optical properties of the crystal in usual circumstances (a plane-parallel sample cut out from the crystal) should not play any significant role in these investigations. It may happen, however, that due to some peculiar effects (defected structure) the angle between e.g. the optical axis and the normal to the sample may vary in sample's plane. In such particular case the birefringence anisotropy can also influence the total **OI** of the investigated sample.

2.3. INFLUENCE OF OPTICAL INHOMOGENEITY OF CRYSTALS ON DEVICE PERFORMANCE

This influence is only fairly well established in nonlinear optics. One of the well known conditions on 80 % theoretical efficiency in second-harmonic generation (SHG) gives

$$\delta(\Delta n) < \frac{\lambda}{4D} \tag{5}$$

where D is thickness of the optical element.

Providing that D is 4 cm and the wavelength used is 1 μm, from eq. (5) one calculates that the birefringence changes should be smaller than 6×10^{-6}. From the previous chapter it can be concluded that this is a rather hard condition to be fulfilled

in real circumstances, since the birefringence content involved by residual stresses only may easily exceed this value.

A few examples illustrating this problem are given below. In elderly works of F.R. Nash et al. [12] and H. Tsuya et al. [13] it is declared that these changes should be smaller than 10^{-4} for SHG in $LiNbO_3$ and $Ba_2NaNb_5O_{12}$, respectively. H. Tsuya [13] has also distinguished between SH power ($\delta(\Delta n)<1x10^{-4}$) and SHG temperature bandwidth ($\delta(\Delta n)<3x10^{-4}$), respectively. A more recent works are also "more severe" for this condition. For example, Yu. Bakhirin et al. [14] came to the conclusion that these changes should be smaller than $1.5x10^{-5}$ for a 45 mm slab of $BaNb_2O_5$, whereas a hard condition of $\delta(\Delta n)<5x10^{-6}$ was placed on $LiNbO_3$ by Z.J. Ivanova et al. [15]. This last value seems to be hard to be fulfilled in larger volumes of $LiNbO_3$ crystals, even those carefully manufactured for optical purposes.

In the book by Y.R. Shen [16] a conclusion has been derived that for practically all nonlinear optical processes this magnitude should be smaller than $2.5x10^{-5}$. The same conclusion can be derived from the work of D. Yu. Sugak et al. [17]. It seems then, that the above mentioned value can be regarded as a figure of merit for nonlinear crystals and nonlinear optical applications.

Less fairly the OI effect is documented on the performance of lasing crystals. There are only a few experimental data published in this subject. In the work of D. Petrova et al. [18] it was observed that the slope efficiency of the output power in YAG:Nd laser rods is resonably smaller in the rods cut out from the parts of the crystals with large birefringence inhomogeneity. It should be noted that such influence was observed in spite of a generally relatively small B from c.a. $5x10^{-6}$ cm^{-1} up to $2x10^{-5}$ cm^{-1}. Similar conclusions can be derived from the cooperative works of Institute of Electronic Materials Technology and the Military University of Technology (Warsaw) [19,20] carried out on $SrLaGa_3O_7$ and YAG:Cr,Tm,Ho laser rods, respectively. Thus a general, but rather trivial conclusion can be made that the best lasing properties are achieved in laser rods cut out from the most optically homogeneous parts of the crystals.

There are no satisfactory experimental (published) data on what exactly is the influence of residual stresses in semiconducting isotropic crystals like Si and GaAs on device performance. A more pronounced are the problems of stresses generated during mounting of a device, like in e.g. Si pellets [21], or during device manufacture, like e.g. during p-n junction formation by the diffusion or epitaxial process [22]. In the "ancient" times of semiconductors' industry cracking of the crystals and plates was a frequent problem and there had been several works published on residual stress formation and/or investigation around the year 1960 [e.g. 23,24]. Due to large improvements in crystal pulling processes and also in mechanical treatment of wafers (cutting, grinding, polishing) this problem had been overcome or greatly reduced in further 10-15 years.

In the last few years, however, an increased interest in residual stress investiga-

tions and mapping carried out on large area semiconducting wafers and an increasing number of papers published in this subject indicates that "something" connected with residual stresses has to play an important role, either in technology or in utilities of the material. The author then believes that there should be a significant influence of residual stresses on the yield and device parameters in VLSI industry, since residual stresses greatly increase with crystals' dimensions, and, besides, that a lot of time (and money) have been spent by many investigators on constructing sophisticated polarimetric arrangements and for investigation of residual stresses, especially in large GaAs wafers.

In conclusion to this chapter the author would like to summarize that optical inhomogeneity testing is of primary importance in (electro)optical and lasing crystals, and an increasing role of such studies has been recently observed in large semiconductor wafers used in VLSI industry.

2.4 EXPERIMENTAL PROBLEMS

There are at least several methods for **OI** testing in transparent materials, among which the prism (or minimum deviation) method, the prism coupling method, the conoscopic method (measuring anomalous biaxiality), the spontaneous parametric light scattering method, the deviation of the coupling angle in SHG, and the polarimetric methods seem to be most frequently used. A good introduction to these and also to some other methods can be found in books by M. Pluta [25] and by F. Ratajczyk [26]. All these methods have certain advantages and disadvantages, some of them require a precise optical instrumentation and the other do not, they also offer different spectrum for measurement conditions (samples' dimensions and finish, wavelength, etc.), hence choosing a specific method for OI testing is a sophisticated problem in itself.

For example, the minimum deviation method [27] offers an opportunity for separate testing of the two refractive indices n_o and n_e instead of birefringence (i.e. n_e-n_o) that is usually measured by other methods. This might be an invaluable feature in certain cases, like in undoped $LiNbO_3$ crystals (see preceding chapter), since it has been discovered that the ordinary refractive index n_o is practically independent on stoichiometry, while a strong dependence on this parameter of the extraordinary refractive index n_e might be then used as a measure of [Li]/[Nb] ratio. Using this method, however, is troublesome: it requires a very precise optical goniometer, a high precision of prism orientation and finish, and besides, the laboriously cutted and polished prisms can not be later used for other practical applications (a destructive method). On the other hand, the polarimetric methods are capable for measuring commercial standard semiconducting (and other) wafers (nondestructive testing) that can be later packed and sold.

Regardless of the method used in practice, it can be classified as a single point (step-by-step) measuring method, a scanning method or an integrational method. The

spread distribution map of a certain parameter (e.g. birefringence) can be acquired in every of the three above mentioned ways. It must be emphasized here, however, that clear differences between these methods require some attention of their user.

The step-by-step measuring methods can be very sensitive, e.g. retardation error as low as $2x10^{-7}$ radians is available in birefringence measurements [28], since carefully selected discrete photodetectors and high quality crystal polarizers can be used in such case. However, such methods are very slow when mapping procedure is applied, and hence, they also offer poor spatial resolution, since not very many sample's points can be investigated in reasonable time. The scanning techniques can be also very sensitive, since they can also utilize carefully selected high quality optical elements. But they are also relatively slow, from c.a. 15 minutes [29] to 12 hours [30] in acquiring input data for calculating birefringence/stress maps in a relatively low number (c.a. 1000) of sample's points.

In case of the so called image integrating (imaging) techniques sensitivity of measurements depends strongly on TV-camera and video frame grabber (VFG) used in polarimetric configurations. This sensitivity is usually low compared with the preceding two groups of methods, since in practical circumstances the cheapest 8-bit VFGs and commercial Si-CCD matrix TV-cameras are used instead of a more sophisticated (e.g. 16-bit VFG and cooled CCD matrix TV) and also much more expensive equipment. The sensitivity is further reduced by using large area sheet polarizers instead of high quality (but small aperture) crystal polarizers, the latter being inadequate for optical mapping of large area samples. The imaging techniques can offer, however, better perspectives regarding speed and spatial resolution. An image of a sample (or precisely speaking - an intensity of light in every point), for example consisting of 512x512 points (pixels) can be recorded by the VFG within a fraction of a second. Regardless of this high speed of acquiring input data, this can also have a positive influence on sensitivity/errors, since it can be fairly assumed that within such short period of time the basic conditions of experiment (temperature, thermal stability of the light source (power and wavelength), thermal stability of electronic circuitry, stability of the power supply, etc.) are much more suitable than in the case of long-lasting measurements.

So, the imaging techniques seem to be unavoidable in commercial inspection of optical and semiconductor materials due to high speed and large reduction of experimental costs, and they seem also very perspective in scientific research work due to high spatial resolution, invaluable in mapping of different parameters on wafer's area.

The forthcoming text is entirely devoted to the imaging polarimeter, i.e. the polarimeter using TV/VFG image integrating technique. Such technique have been chosen for quick and nondestructive testing of wafers, especially of semiconducting and oxide crystals manufactured by the ITME. The nondestructive testing is of primary importance in complementary research works, when the same wafer is later (or earlier) studied by other methods (e.g. photoluminescence, optical spectroscopy, X-ray techniques, etc.).

3. PRINCIPLES OF THE METHOD

In earlier work [1] it was shown, that intensity of a parallel light beam after passing through a linear polarizer, a birefringent plate characterized by retardation δ, and another linear polarizer (the analyzer) whose transmission axis is set at an angle of 45° versus the first polarizer, and detected by a linear photodetector is given by

$$I = kI_o T_r\left[1 + \tfrac{1}{2}(1 - \cos\delta)\sin 4(\alpha - \theta)\right] \tag{6}$$

where I is signal of the detector, k is constant comprising transmissions of both polarizers and sensitivity of the detector, I_o is intensity of light incident on the polarizer, T_r is transmission of the plate, α is the polarizer's angle versus the base of the arrangement (the analyzer's angle is α-45°), and θ is the principal azimuth of the retarder (the plate). The angles are measured versus the base of the arrangement (the horizon) in the counterclockwise direction when looking from the detector towards the light source. At least three measurements are needed to determine the three unknowns from eq. (6), i.e. kI_oT_r, δ and θ.

From eq. (6) it follows, that the intensity I resembles, a shifted sinusoidal function of the quarternary argument (α-θ), the period of which is equal to 90°. To solve this equation for the three unknowns it is then necessary to record the first picture of the sample (record I at every investigated pixel), next to rotate simultaneously the two polarizers versus a fixed sample by an incremental angle of 30° (1/3 of a period) and record the second picture, and repeat this procedure for the third time. By analysing different measurement procedures in [1] it was concluded, however, that the above described the so called three-intensities (or three bucket) technique is more erroneous than other techniques using four or even five intensities' records. Therefore after a critical analysis of this problem the author has chosen the so called four-intensities or Carré method, i.e. the method using four intensities' records by applying an incremental angle unequal to the even division of the period (90°/4=22.5°). Using the even division of the period (the Wyant's method) would be in this particular case of the polarimeter troublesome (although technically possible) from the point of view of the stepper motor's operation.

The measurement procedure starts then with the polarizer's angle α equal to zero (the polarizer's transmission axis is parallel to the horizon) and next this angle is three times incremented by the constant angle ψ equal to 22°. This yields four equations for the intensity of the transmitted light

$$I_1 = kI_o T_r\left[1 - \tfrac{1}{2}(1 - \cos\delta)\sin 4\theta\right] \tag{7}$$

$$I_2 = kI_o T_r\left[1 + \tfrac{1}{2}(1 - \cos\delta)\sin 4(\psi - \theta)\right] \tag{8}$$

$$I_3 = kI_oT_r\left[1 + \tfrac{1}{2}(1 - \cos\delta)\sin 4(2\psi - \theta)\right] \tag{9}$$

$$I_4 = kI_oT_r\left[1 + \tfrac{1}{2}(1 - \cos\delta)\sin 4(3\psi - \theta)\right] \tag{10}$$

From these equations it is possible to determine all the three unknown quantities, i.e.

$$kI_oT_r = \frac{(I_1I_3 - I_2I_4)\sin 8\psi + (I_3I_4 - I_1I_2)\sin 4\psi}{(I_2 - I_3)(\sin 12\psi - \sin 8\psi - \sin 4\psi)} \tag{11}$$

$$\cos\delta = 1 - 2\eta\frac{(kI_oT_r - I_1)\sqrt{1 + \left(\frac{L}{M}\right)^2}}{I_o\frac{L}{M}} \tag{12}$$

where $L=(kI_oT_r-I_1)\sin 12\psi$, $M=I_4-kI_oT_r-(I_1-kI_oT_r)\cos 12\psi$, and η is sign of the quotient L/M,

$$\theta = \psi - \tfrac{1}{4}y - \tfrac{3}{8}\pi + m\pi \tag{13}$$

where m is an integer chosen in such way as to yield θ between 0 and $\pi/2$ radians, and $y=\arccos((1-I_2/kI_oT_r)/0.5(1-\cos\delta))$.

3.1 PROCEDURES USED FOR TRANSMISSION, BIREFRINGENCE AND THE PRINCIPAL AZIMUTH MAPPING

Transmission, phase retardation and the principal azimuth can be calculated from eqs. (11), (12) and (13), respectively, since the same data are also acquired for the background, i.e. the background transmission and phase retardation is being measured without a sample. In the case of bacground kI_oT_r in eq. (11) equals to kI_o as no sample is inserted, hence by a suitable division T_r is easily obtained in absolute (%) units. The background modulation pattern theoretically equal to zero, and in practice unequal to zero due to some parasitic phenomena (partial plane-polarization of the light source, imperfections of both polarizers, electronic noise in the TV-camera/VFG system) is equivalent to a false (or background) retardation and as such it can be subtracted from retardation measured afterwards with a sample inserted in its compartment.

Two additional comments have to be made here on the above formulas. Equation (11) being a precise formula from the arithmetic point of view can, however, yield erroneous results in practical VFG systems where some output noise can be expected. From this equation one can easily imagine that in the case of small retardations two minor quantities can be divided by each other or even a division by zero can be

expected. In such case the right-hand side of eq. (11) can be replaced by $(I_1+I_2+I_3+I_4)/4$ - a formula being a good approximation of the original one for small retardations. Besides, eq. (12) derived directly from eqs. (7) to (10) can be further simplified to give

$$\cos\delta = 1 - 2\left(1 - \frac{I_1}{kI_oT_r}\right)\sqrt{1+\left(\frac{L}{M}\right)^2} \qquad (14)$$

and it can be also showed that this formula yields less erroneous results than eq. (12). It is a specific feature of systems like VFGs and also others not free from output noise that equivalent equations can issue different results, especially when the input data are close to zero (or to infinity).

Transmission mapping presents no particular problems, since, as it has been noted above, a kI_oT_r/kI_o division yields directly T_r in [%] units.

There are, however some peculiarities in birefringence mapping that need to be remarked here. As is seen from eq. (3) the phase retardation (the cosine of it is directly measured by the polarimeter) equals $2\pi d(n_e-n_o)/\lambda$. The larger is thickness of the wafer d, or the shorter is wavelength λ, the larger is δ. It can be either equal to zero (zero-order retardation) when $n_e-n_o=0$, or it can be positive or negative. Since a cosine of retardation is being measured one can not simply distinguish whether δ is positive or negative, i.e. the automated mapping method is not capable to recognize between positive and negative birefringent crystals, or between compressive and tensile residual stresses in the case of isotropic materials. In the latter case it may happen that two (or more) stressed regions differing in sign can occur in the same crystal (a frequent case in YAGs grown with a core where residual stresses have opposite sign in the core versus the remaining part of the crystal [e.g. 31]). In such case no any indication of areas differing in retardation (birefringence) sign can be found on adequate maps.

The second problem associated with retardation/birefringence mapping comes out from the order (orders) of retardation met in practice. The zero-order retardation can be experienced in two practical cases: on a sharp border between two regions differing in stress signs, and in a relatively broad region of the crystal (wafer) where difference of the two principal residual stresses equals zero as a consequence of the absence of stress. The latter case can be found in practice in wafers cut out perpendicularly to the growth direction of Czochralski-grown crystals. From theory of residual stress generation in such crystals [e.g. 32] it follows that the difference of radial and tangential principal residual stresses increases from zero at the center to a maximum at the perimeter of the crystal. In practical circumstances, however, this zero is not a single point value (as it should be) and due to limited sensitivity of the polarimeter and to some other effects, a broader region indicating a zero-order retardation is frequently observed in samples cut out perpendicularly to crystals' axes.

From the same theory [32] it also follows that the difference of the axial and radial principal residual stresses changes its sign somewhere between the center and the perimeter, i.e. two sharp zero-order retardation borders parallel to crystal's axis should be seen in samples cut parallely to the growth direction of Czochralski-grown crystals.

To conclude this problem it should be said, that the birefringence maps calculated by the computer should be then read very carefully by the user, who also ought to acquire some knowledge regarding physics of crystal growth processes. A narrow region (line) of zero-order retardation usually indicates change in sign between two oppositely stressed regions of the crystal (material), whereas an adequate broader plane should be equivalent to a stress-free region.

The third problem is connected with multiple orders of retardation. If retardation is of a non-zero order it can be either fractional (i.e. $\delta < 2\pi$), or of the 1-st order ($\delta = 2\pi$), or of the multiple orders ($\delta = 2m\pi$, $m = 2,3,...$). δ can also owe some intermediate values (e.g. $\delta = 2.3\pi$). Since $\cos\delta$ is a periodic function one can not easily distinguish between δ being equivalent to the 1-st or to any higher order of retardation, and so it is also in the case of a fractional value (e.g. $\delta=\pi/2$) and some intermediate values ($\delta = 2\pi+\pi/2$, $4\pi+\pi/2$, etc.). It is a serious problem and it can either practically arise (see notes at the beginning of this chapter) in thick samples of nonbirefringent materials (retardation involved by residual stresses is usually low) or in any practically met samples of birefringent crystals. For example, assuming wavelength to be 1 μm and birefringence $8.5\text{x}10^{-2}$ ($LiNbO_3$) it can be easily calculated that even such thin (and practically unrealizable) samples with thicknesses like 12 μm can yield retardations greater than 2π. In practical cases of 0.5 mm thick $LiNbO_3$ wafers orders of retardation between 38 and 45 can be experienced depending on birefringence of the crystal. In such cases a special technique using different wavelengths [1] has to be used to reduce uncertainty of birefringence (retardation) estimation. Nevertheless, this uncertainty still remains and so the author after a one year experience in using the polarimeter in automated birefringence mapping have quitted this troublesome and laborious method, and further practice has shown that in order to acquire precise retardation (birefringence) data one should use Z-oriented (perpendicular to the optical axis) birefringent samples and thin or moderately thick (even a few to 10 mm thick) samples of nonbirefringent materials.

The problem of the principal azimuths (or the principal residual stress directions) mapping has been solved in accordance with eq. (13). To increase readibility of such maps one of the azimuths have been quitted (the two azimuths are perpendicular to each other), and only the first principal azimuth is then plotted. The integer m in eq. (13) is chosen by the computer in such a way as to yield θ always between 0 and 90°, and for a typical radial residual stress distribution the principal azimuth map should resemble a spokes-of-the-wheel-like pattern.

All the maps can be plotted either in 2-D (plane map) or 3-D versions. The grey-shaded versions (either positive or negative) and any parallel or perpendicular cross-sections are also available.

3.2 RESIDUAL STRESS MAPPING

In certain circumstances residual birefringence maps are insatisfactory, e.g. in residual-stress studies of crystals grown by different techniques. However, calculation of residual stresses from birefringence (retardation) data is a complex problem in itself. There are at least several ways to solve this problem in samples owing a shape of a thin disc (a wafer), of which the procedures presented by Yamada for GaAs [30] and by Koechner and Rice for YAG [33] are worth noting here. Using thin samples in the procedure of stress measurement/mapping is a convenient way of solving this problem, since it can be then fairly well assumed that there are only two stress components active in the sample (in sample's area), and that the third stress component perpendicular to it is absent (or nonactive).

In this work a simple procedure of transformations performed on adequate matrices to yield the final result is presented below. Two cases of such transformations having practical importance are considered : transformation of the primary [x,y,z] Cartesian coordinate system to another one [x',y',z'], and the same procedure later followed by rotation of this Cartesian [x',y',z'] system to [r,t,s] cylindrical coordinates (a simple rotation around e.g. z' axis in the (x',y') plane). These transformations/rotations are very useful, since piezooptical coefficients of different materials listed in literature are usually not transformed to novel coordinates used in practice. The first procedure is used when the sample owing a shape of a thin (quasi)rectangle is being cut out parallely to the growth axis of the crystal. The second one is used in the case when the crystal is pulled in another than the z-crystallographic direction, and next the sample owing a circle-like shape is being cut out perpendicularly to this direction. In the case of such circular samples it is convenient to introduce cylindrical coordinates and to transform the principal residual stresses in the [x',y',z'] coordinates to the new cylindrical ones.

Imagine then that the Cartesian crystallographic [x,y,z] axes are transformed to the new system of Cartesian coordinates [x',y'z']. The relation between the new and the old system will be

$$\begin{bmatrix} x' \\ y' \\ z' \end{bmatrix} = [c] \begin{bmatrix} x \\ y \\ z \end{bmatrix} \tag{15}$$

where [c] is a 3x3 square (2nd rank) matrix of adequate cosines of the angles between the "new" and the "old" axes, respectively. An opposite rotation, i.e. from the new to the old system of coordinates gives

$$\begin{bmatrix} x \\ y \\ z \end{bmatrix} = [c^T] \begin{bmatrix} x' \\ y' \\ z' \end{bmatrix} \tag{16}$$

where $[c^T]$ is an adequate transpose of [c].

Imagine next, that a circular plate (wafer) is being cut out perpendicularly to the z' axis in the new system of coordinates (note that z' is not necessarily the direction of the optical axis in general case), and that the stresses acting in the (x',y') plane are described in the cylindrical system of coordinates, hence

$$\begin{bmatrix} r \\ t \\ s \end{bmatrix} = [a] \begin{bmatrix} x' \\ y' \\ z' \end{bmatrix} \tag{17}$$

where [a] is an adequate rotation matrix given by the formula

$$[a] = \begin{bmatrix} \cos\phi & \sin\phi & 0 \\ -\sin\phi & \cos\phi & 0 \\ 0 & 0 & 1 \end{bmatrix} \tag{18}$$

where ϕ is an angle between the x' and r ("r" denotes "radius") axes. An opposite rotation yields

$$\begin{bmatrix} x' \\ y' \\ z' \end{bmatrix} = [a^T] \begin{bmatrix} r \\ t \\ s \end{bmatrix} \tag{19}$$

where $[a^T]$ is a transpose of [a]. It is worth noting here that the (scalar) multiplicant of $[a][a^T]$ or $[a^T][a]$ results in a unit diagonal matrix.

The stress tensor described in the cylindrical system of coordinates is next transformed to the Cartesian system [x',y',z'] (see e.g. J.F. Nye [6] for the rules of such transformations)

$$[\sigma_{(x',y',z')}] = [a^T][\sigma_{(r,t,s)}][a] \tag{20}$$

and later to the primary [x,y,z] Cartesian system

$$[\sigma_{(x,y,z)}] = [c^T][\sigma_{(x',y',z')}][c] = [c^T][a^T][\sigma_{(r,t,s)}][a][c] \tag{21}$$

It has to be emphasized here that notations like e.g. $\sigma_{(x,y,z)}$ do not mean that σ has only three components along x, y, and z directions. In fact it is a 2 nd rank tensor and the above notation only means that it is described in the proper system of coordinates.

The stresses through the piezooptical effect [6] will involve a change in the dielectric impermeability tensor (see chapter 2.1), i.e.

$$[\Delta B_{(x,y,z)}] = [\pi_{ij}][\sigma_{(x,y,z)}] = [\pi_{ij}][c^T][a^T][\sigma_{(r,t,s)}][a][c] \tag{22}$$

where $[\pi_{ij}]$ is a 6x6 square (4th rank) matrix of the piezooptical coefficients of a

material. The inverse transformations of [ΔB] yield

$$\left[\Delta B_{(x',y',z')}\right] = [c]\left[\Delta B_{(x,y,z)}\right][c^T] = [c][\pi_{ij}][c^T][a^T]\left[\sigma_{(r,t,s)}\right][a][c][c^T] \tag{23}$$

and

$$\left[\Delta B_{(r,t,s)}\right] = [a][c][\pi_{ij}][c^T][a^T]\left[\sigma_{(r,t,s)}\right][a][c][c^T][a^T] \tag{24}$$

Equation (24) can be also rewritten in a more contracted form as

$$\left[\Delta B_{(r,t,s)}\right] = [k_1][\pi_{ij}][k_2^T][a^T]\left[\sigma_{(r,t,s)}\right][k_1][k_2^T] \tag{25}$$

where $[k_1]=[a][c]$, $[k_2]=[c][a]$, and index T denotes a proper transposition operation.

Next we assume that the plate is cut out perpendicularly to the z' or s direction and that it is thin enough so only the two stress components σ_r (radial) and σ_t (tangential) are non-zeroed. In such case the index ellipsoid (see chapter 2.1) will be contracted to an ellipse in the (r,t) plane with its axes parallel to the r and t directions, respectively. Denoting the refractive indices by n_1 and n_2 along the r and t directions, respectively, one obtains

$$\Delta B_r - \Delta B_t = \frac{1}{n_1^2} - \frac{1}{n_2^2} = \frac{(n_2 - n_1)(n_2 + n_1)}{n_1^2 n_2^2} \tag{26}$$

where ΔB_r and ΔB_t are the adequate components of [ΔB].

Next it comes the same simplification as done by "everybody in the world", i.e. it is assumed that $n_1 = n_2 = n_o$ (the refractive index for an unstrained material), and hence from eq. (26) it follows that

$$\Delta B_r - \Delta B_t \approx \frac{2}{n_o^3}\Delta n \tag{27}$$

Before continuying this chapter the author would like to make a comment on eqs. (26) and (27). For such materials as e.g. $LiNbO_3$ it can be easily calculated that difference between the two equations may reach c.a. 0.2 % (see Appendix A) or even more in highly stressed crystals or crystals with larger unstrained refractive index n_o. It seems to be not much, but, however, one has to keep it in mind that besides numerous other errors this is an additional error in stress determination. Unfortunately, one is not able to use the proper eq. (26) in practical calculations, since no such combination of the refractive indices as that on the right hand side of this equation is available from experiments.

From eqs. (27), (25), and (18), it can be concluded that the difference of ΔB_r and ΔB_t can considerably depend on angle ϕ, and, moreover, it may not be a function of any simple combination of σ_r and σ_t (e.g. σ_r-σ_t). It is an interesting phenomenon that this last feature met frequently in practical configurations of crystalline samples is

often neglected (or unrecognized) by many investigators who believe that the stress-induced birefringence in thin plates is always proportional to the difference of these principal stresses. Another investigators, especially those who try to derive themselves the adequate formulas, make necessary simplifications to yield a simple relation between Δn and $(\sigma_r - \sigma_t)$, of course at a cost of additional errors.

If no rotations are performed in the (x',y') plane then it can be shown that

$$\left[\Delta B_{(x',y',z')}\right] = [c][\pi_{ij}][c^T]\left[\sigma_{(x',y',z')}\right][c][c^T] \tag{28}$$

and eq. (27) also holds in this case.

Also, if no transformations from [x,y,z] to [x',y',z'] Cartesian coordinate system is done, and only rotation around the normal to the plate's (wafer's) area is performed in the [x,y,z] system itself, then

$$\left[\Delta B_{(r,t,s)}\right] = [a][\pi_{ij}][a^T]\left[\sigma_{(r,t,s)}\right][a][a^T] = [a][\pi_{ij}][a^T]\left[\sigma_{(r,t,s)}\right] \tag{29}$$

where [a] is an adequate rotation matrix (eq. (18) holds for rotation around crystallographic z axis).

In Appendix B two cases of residual stress mapping in $LiNbO_3$ from birefringence (retardation) data, i.e. $LiNbO_3$ plates cut out perpendicularly to the Z-growth direction (no Cartesian transformation, only rotation in the Z-plane around the Z (optical) axis), and plates cut out parallely to the growth Y-axis (neither transformations nor rotations), are considered. For more complicated transformations/rotations (e.g. <100> oriented circular GaAs wafers [30] or <111> oriented YAG [33] (the analysis and formulas are also valid for <111> oriented Si) the reader is encouraged to be acquainted with cited works.

At the end of this chapter the author would like to summarize that :

1) Error for the stress-induced birefringence (as measured) is always lower than for the corresponding residual stresses (when calculated from birefringence/retardation data).

2) There are several reasons for which the user of the method and arrangement should take care when dealing with the residual stresses maps instead of the corresponding birefringences:

a/ uncertainty of the piezooptical coefficients' determination by different investigators. This problem has not been yet discussed in this work but it is the main problem of stress determination from birefringence measurements. Unless somebody is lucky enough to have its own apparatus for determination of the piezooptical (or photoelastic) coefficients, he has to use adequate data from the worldwide literature. There is no room for further discussion of this problem here, but a few unexpected and rather unpleasant phenomena can be experienced when "digging through" published papers on this subject;

- there are no published data on (especially) new materials,
- there might be only one paper for a specified material, sometimes published 30

or more years ago,

- there are discrepancies in the data published by different investigators not only regarding the absolute quantity of a specified coefficient but sometimes also its sign (!),
- a measured set of coefficients is frequently limited to only a few of them, e.g. π_{11}-π_{12} and π_{44}, being insatisfactory for many practical configurations (orientations) of the material in use.

b/ The so-called "piezooptical constant" (also the "photoelastic constant") as it is described in the literature is not a constant, in fact, and so the author uses here the term "piezooptical coefficient". As everybody can easily imagine these coefficients are functions of several parameters, the main being wavelength of the light beam, doping of the material and temperature. It is also expected that structural perfection of the material plays also an important role, and hence the data published 30 or 40 years ago should be read very carefully (how to do it when these are the only data available in some cases ?). The dependence of π_{ij} on wavelength is also sometimes neglected by people using published data acquired from e.g. He-Ne laser radiation in another parts of the spectrum.

c/ In the majority of material's orientations versus the light beam direction through it the relation between birefringence and (usually) the difference of the principal residual stresses is not directly proportional, and hence the necessary simplifications yield adequate errors (some of them have been discussed in this work).

d/ Sometimes instead of the piezooptical coefficients π_{ij} the so-called photoelastic coefficients (or constants) p_{ij} are being measured and their values published in the literature. If stress rather than strain maps are of the main interest, then a new problem arises due to the fact that piezooptical coefficients are related to photoelastic coefficients by the so-called stiffness coefficients s_{ij}. If the data on stiffness coefficients of the material are available from the literature then only some additional errors arise due to uncertainty of their determination by different investigators and/or by different methods. If not, then the user of the arrangement is unable to plot residual stress maps, and only residual strain maps will be available to him.

3) If it would be only possible to use residual birefringence maps instead of the residual stress maps then it is highly advisable to do so. In all possible circumstances the birefringence maps will be much more close to reality than the stress maps, and, besides, one does not need to laboriously calculate the relations between birefringence and stresses or to use published formulas, often simplified without any notice.

4. ARRANGEMENT

A block diagram of the arrangement is shown in fig. 1, whereas its general and enlarged fragments in figs. 2 and 3, respectively.

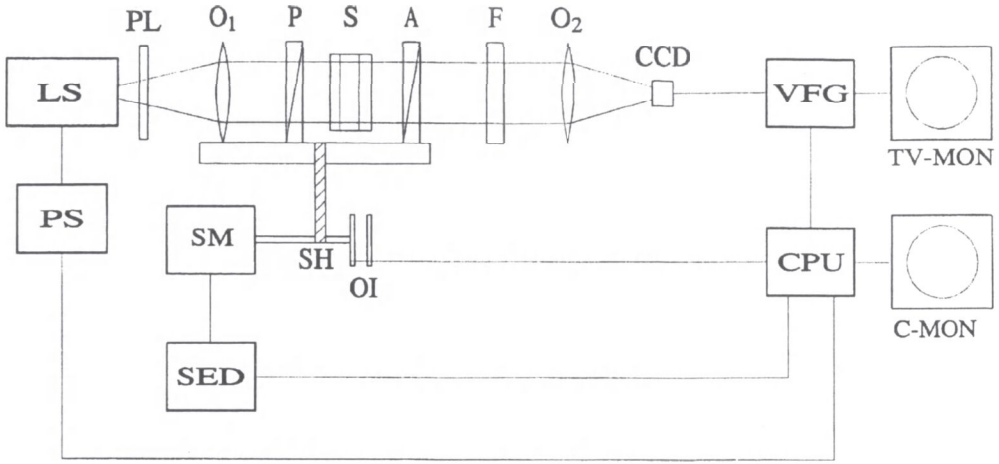

Fig. 1. Block diagram of the arrangement.

The arrangement described in details in [2] consists of a 24V/150W halogen lamp, a depolarizer composed of two polyethylene plates, a condensor system for producing a parallel beam of light, a pair of HR-type sheet polarizers, a set of seven interference filters (fig. 3) in the wavelength range from 676 to 1080 nm (the TV camera's cutoff wavelength without a filter is approximately equal to 1150 nm) and a Si CCD TV-camera and 8-bit VFG detecting system. The sample itself is placed in a specially designed mount (fig. 4) constructed in such a way as to exert a negligible tension on it [2].

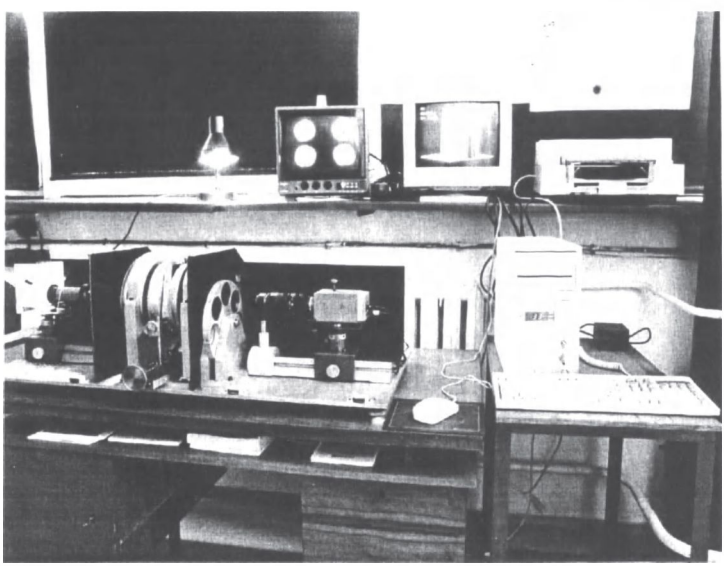

Fig. 2. General view of the arrangement (polarimeter with unmounted cover) comprising TV- camera's monitor (upper left), computer's monitor (upper middle), deskjet printer (upper right), polarimeter (bottom left), and IBM 486 33-MHz computer. The four measured sample's images are displayed on the TV-camera's monitor, whereas the calculated map is presented on the computer's monitor.

The transmission axes of the polarizers can be set versus each

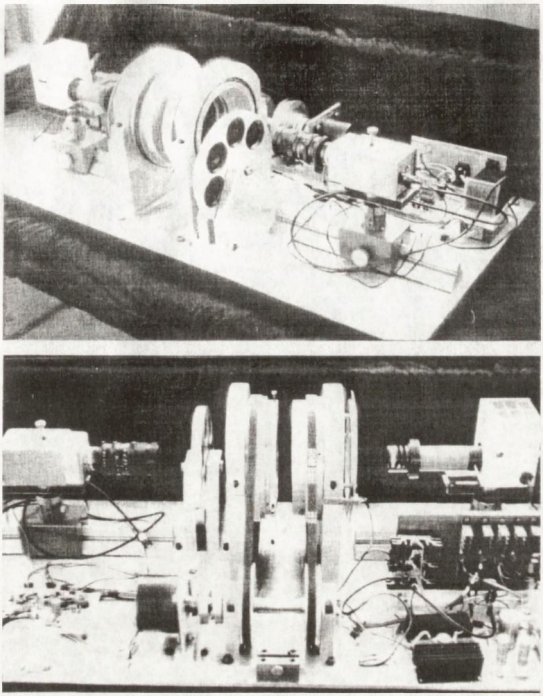

Fig. 3. Polarimeter with unmounted cover and sidewalls viewed from the front (upper picture) and from the rear (bottom picture).

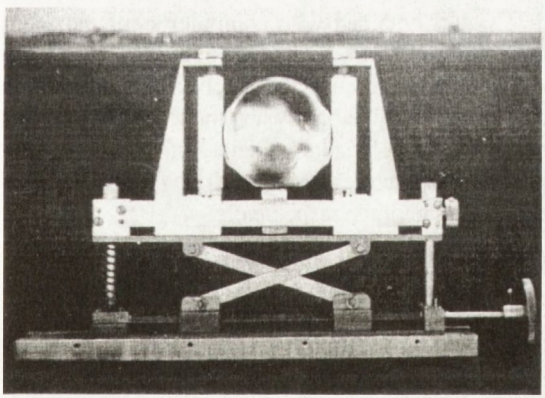

Fig. 4. Sample's munt holding a 4", 10 mm thick Si slab.

other at 0° (parallel polarizers), at 45° (measurement mode) or at 90° (crossed polarizers). The parallel and crossed polarizers options characteristic for the plane-polariscope operation are used for observing samples' images. These options can be very useful in certain circumstances, since in the parallel polarizers configuration one can usually observe dark isochromatic lines of the odd orders of retardation (π, 3π, 5π, etc.) on sample's bright area, whereas in the crossed polarizers configuration dark isochromatic lines of the even orders of retardation (0, 2π, 4π, etc.) are usually seen together with dark isoclinic lines, the latter lying along directions of residual stresses. Following the remarks presented in chapter 3.1 it becomes clear that the plane-polariscope configuration is very useful for checking what the order of retardation(s) really is. It is no place to discuss it widely here, but the reader may believe the author that it is not a complicated problem to find out whether the maximum retardation in a plate is exceeding 2π or not, i.e. to decide whether the birefringence maps calculated by the computer (always between the limits of retardation between 0 and 2π) are correct. The plane-polariscope configurations are also very useful for demonstration and tuitorial purposes. For example, in thin isotropic samples no isochromatic lines corresponding to other than the zero order retardation line can be usually visible (fig. 5) , and hence all the remaining dark lines on sample's bright area should be the isoclinic lines, which can quickly demonstrate symmetry of residual

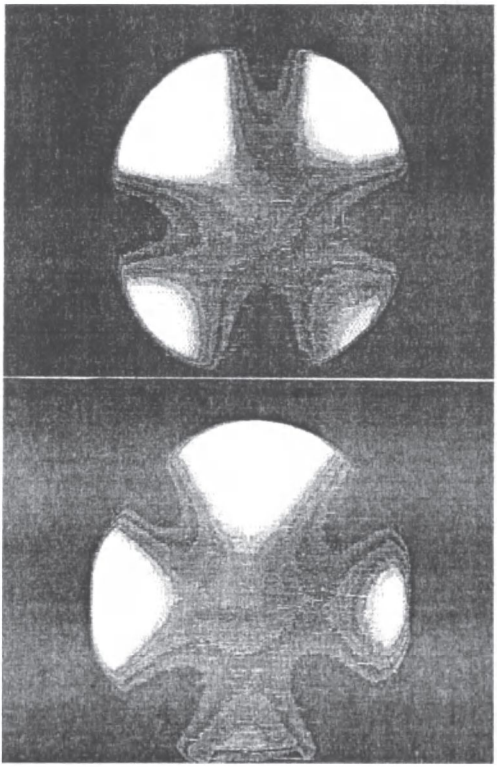

Fig. 5. Plane polariscope pictures (crossed polarizers) of a Z-oriented (optical axis), 4" diameter $LiNbO_3$ wafer. Rotation of dark isoclinic cross (by 45° on the bottom picture) involved by the adequate rotation of both polarizers' transmission axes is an indication of radial distribution of the principal azimuth (radial residual stress direction). No other isochromatics than that of the zero-order retardation (center of the cross) can be deduced from both pictures.

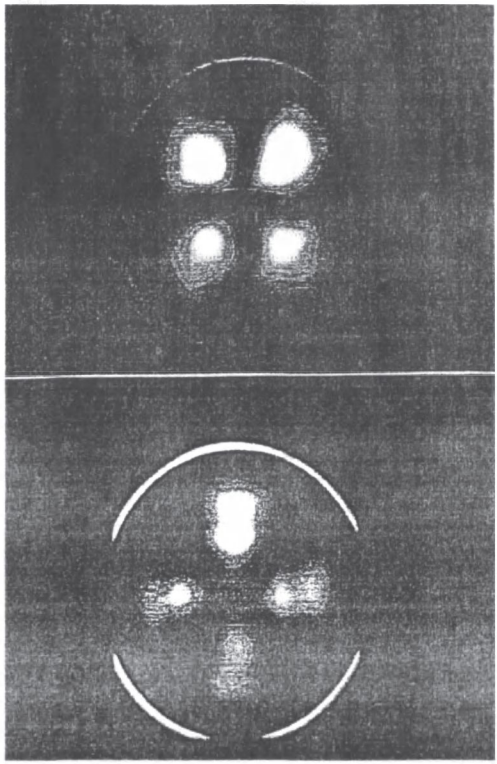

Fig. 6. Plane polariscope pictures (crossed polarizers) of a <100> oriented, 3" diameter GaAs wafer obtained with computer's enhancement of the contrast. In the case of anisotropic <100> oriented samples the isoclinic black cross is clearly visible only when the transmission axes of both polarizers coincide either with <010> (upper picture) or with <011> (bottom picture) directions, respectively.

stress distribution. Quality of such printed pictures, as e.g. that presented in fig. 5, is usually low compared to normal photos, and hence, a computer enhancement of the output pictures is sometimes used (fig. 6) for eliminating any doubt of whether a specified line is an isoclinic or an isochromatic.

In both parallel and crossed polarizers configurations the transmission axes of the polarizers can be rotated either clock or counterclockwise versus an immobile sample by a four-phase stepper motor (fig. 3 - bottom picture) by clicking appriopriate keys on the computer's keyboard.

In the polarimetric (measurement) mode the angle between the transmission axes of the polarizers is set at 45° and the operation follows the procedure described in chapter 3, i.e. the measurement always begins with the polarizer's transmission axis parallel to the horizon, and next it is thrice incremented by the constant angle of 22°.

Before closing this chapter a few more remarks have to be made here :

1) a special procedure can be applied as an option for eliminating random noise (the so called unwrapping is using a low-pass Gaussian filtering).

2) the final input data (I_1, I_2, I_3, I_4) can be averaged from multiple measurements. In the previous version of the computer's program [1] a certain backslash of the stepper motor was assumed, and hence an algorithm averaging the input data in multiple rotations was applied. Since no evidence of any backslash has been later found the averaging procedure was then changed in the present version of the program. Only one rotation is applied and averaging is done immediately after each incremental change of the polarizer's transmission axis. Such change of the procedure yielded in a considerable decrease of the operation time. For example, using 10 averaging cycles consumes less than 43 seconds to record (and average) all the four images, and then further 6-7 seconds for calculating an appropriate map.

3) the maximum number of averaging cycles is given by the formula (65536/2 -1)/ 256=127 where integer 256 corresponds to the maximum grey (or white) level in the 8-bit VFG system. Providing that the maximum intensity of light in every pixel is lower than 255 then the number of averaging cycles can be adequately increased over 127.

5. SENSITIVITY AND ITS OPTIMIZATION

A detailed error analysis and modelling had been performed in earlier work [1]. On the basis of theoretical calculations it was concluded that the retardation error/ sensitivity of 4×10^{-3} radians, corresponding to birefringence error/sensitivity of 5×10^{-7} for 1 mm thick sample and 0.8 μm wavelength could be reached even in an 8-bit VFG system providing that random errors are eliminated or greatly reduced. These random errors are mostly concerned with electronic noise in the camera/VFG detecting system and it was believed that they could be eliminated in practice by suitable averaging the input data from multiple measurements.

The transmission error was estimated to be lower than 1 % of the peak value in any circumstances and it seems to be a satisfactory result for general purpose transmission mapping.

The principal azimuth error usually smaller than a fraction of a degree (1.7×10^{-2} rad) is, however, undetermined for retardations equal exactly to 0, 2π, 4π, etc., i.e. when no modulation occurs at all (see eqs. (7) to (10)). Nevertheless, even in such circumstances no "empty holes" are printed by the computer's program on the principal azimuth map.

A comment has to be made here, however, on the above mentioned retardation error/sensitivity. Since measurements are performed on every second pixel, i.e. in a matrix of 256x256 pixels (65536 pixels), it is rather obvious that apart of any averaging or filtering (unwrapping) procedures applied it would be practically impossible to achieve such sensitivity in exactly each of 65536 pixels (sample's points). The reason for that might be imperfections in the CCD matrix itself, an incidental shot noise, imperfect polarizers, and a couple of other reasons. Therefore a retardation error like $4x10^{-3}$ radians means that this is the most probable result for the "great majority" of pixels and the entire map itself. In a few pixels, however, i.e. in a negligible fraction of their total number this may not work at all. Fortunately, depending on the filtering parameters such "hot spots" can be almost entirely eliminated from the map.

A few experiments have been performed in order to optimize the measurement procedure for maximum sensitivity/minimum errors. In the first experiment no influence of whether the power supply was unstabilized (i.e. the voltage was directly supplied from the mains) or stabilized (apart of stabilizing circuitry of the TV-camera itself an additional UPS was used) have been found. Nevertheless, the additional stabilizer was used in further experiments.

A more important experiments were connected with averaging the results in multiple measurements. To illustrate the influence of such averaging on birefringence (retardation) measurements several plots are shown in fig. 7. A continuous (pointed) curve on the left shows time oscillations of the maximum residual retardation of the background (in arbitrary units) measured with only one cycle (no averaging at all), i.e. with no sample in its compartment. Since no particular attention had been payed to the position of a pixel where this maximum occurred (i.e. the maximum not necessarily should occur in the same pixel everytime), such large oscillations might be to some extent a result of "travelling" of this maximum on CCD's matrix area. Nevertheless, it is believed that the primary reason for such large oscillations is connected with no averaging of the input data.

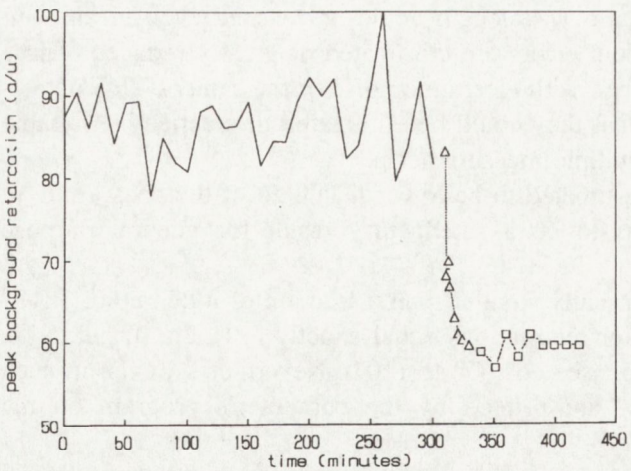

Fig. 7. Time oscillations of the maximum residual retardation recorded on the background :

- pointed curve has been measured with one cycle only (no averaging of the input data),
- curve marked with triangles denotes increase of averaging cycles from one (upper triangle), through 2, 4, 8, 16, 32, 64, respectively, up to 127 cycles (bottom triangle),
- curve marked with squares denotes adequate time oscillations for 127 averaging cycles.

A considerable decrease of the background maximum retardation with increased number of averaging cycles is shown in this figure by a line marked with triangles (the successive bottom-forwarded triangles correspond to an increased number of averaging cycles). Also very important are minor time oscillations of this maximum when a large (127) number of averaging cycles is applied (a curve marked with squares in fig. 7).

To further analyze the results shown in fig. 7 and also from some other measurements the author has introduced the following parameters : δ_{av} (average retardation) - an average from more than 10 measurements (for a specified number of averaging cycles), Δ_{max} (module of the maximum deviation) - the module of the maximal difference between any result and δ_{av} (for a specified number of averaging cycles), s.dev. (standard deviation) - calculated from a classical formula, and the latter two parameters in relation to δ_{av} (in [%] units). The results are presented in table 1 which also includes the input data acquisition time (in seconds) necessary to collect these data (I_1, I_2, I_3, and I_4) from four image captures.

Table 1. Influence of the number of averaging cycles on accuracy of retardation measurements (data acquisition time also included).

Number of averaging cycles	∂_{AV} (a.u.)	S. dev. (a.u.)	Δmax (a.u.)	$\frac{\text{S. Dev}}{\partial_{AV}}$ (%)	$\frac{\Delta \text{ max}}{\partial_{AV}}$ (%)	Data acquisition time (s)
1	87,38	5,14	11,26	5,87	12,88	12
4	69,63	2,09	3,28	3,00	4,72	23
16	62,25	1,76	2,78	2,83	4,46	64
127	59,29	1,17	2,37	1,97	4,00	448

As is clearly seen from this table a much greater reduction of the standard deviation than of the maximum deviation itself is achieved with an increased number of averaging cycles. Such statement supports the author's earlier conclusion that even a considerable number of averaging cycles is unable to cancel gross errors in exactly every of the 65536 pixels. Nevertheless, a noticable and continuous decrease of the standard deviation means that the entire map is free from greater errors in such case.

Since the measurements carried out at a single point (pixel) and, besides, not necessarily at the same point everytime can be somewhat misleading, another set of experiments had been performed. A background measured with 256 averaging cycles have been regarded as a standard (master) for the same background but later measured with a decreasing number of averaging cycles : 127, 16, 4, and 1 cycle,

respectively. In every case the background maps have been calculated on the assumption of a 10 mm thick "sample" (an approximately 10 mm thick air-layer is in-between the two polarizers), and the 975 nm interference filter was used in these investigations. Next, the remaining backgrounds (or precisely speaking - the same background but measured with lower number of averaging cycles) have been treated as "samples", and the standard background was then regarded as a true background for all these "samples". figs. 8, 9, and 10, respectively, show four such "samples'" birefringence, transmission and the principal azimuth maps corrected for the (standard) background, i.e. when e.g. transmission map of any background "sample" is then divided by a transmission map of the standard.

A clear influence of the number of averaging cycles can be concluded from the

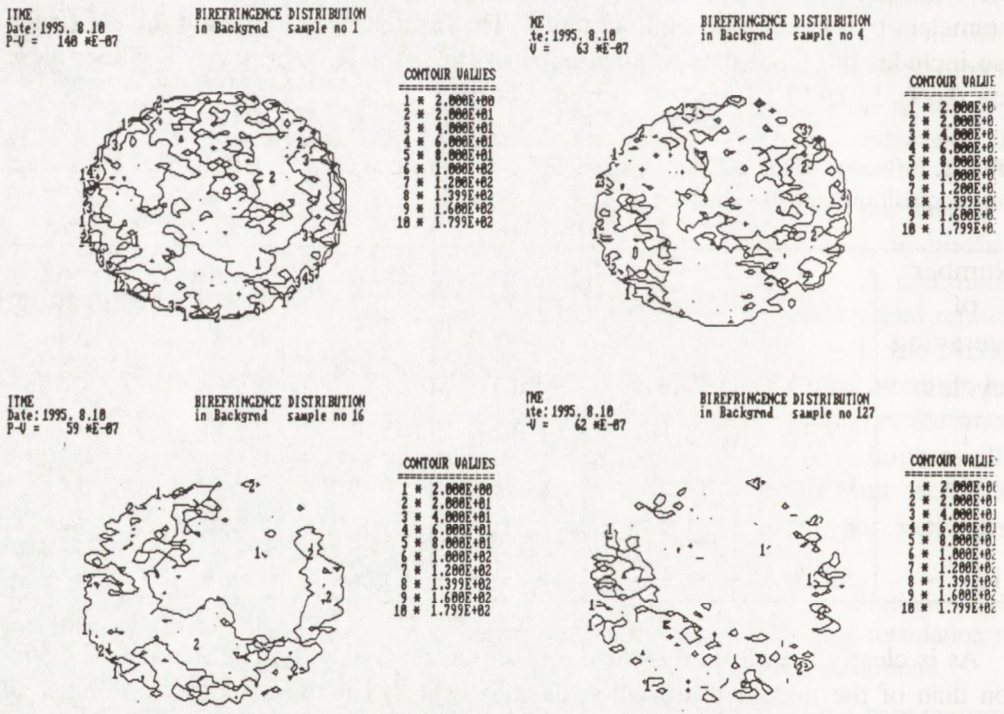

Fig. 8. Residual birefringence distribution of the background corrected for the same background measured with 256 averaging cycles. The appropriate "sample numbers" correspond to actual value of averaging cycles, i.e. one cycle (top left map), 4 cycles (top right), 16 cycles (bottom left), and 127 cycles (bottom right).

four birefringence maps presented in fig. 8. All these maps are plotted in the same scale so that density of the contour lines can be a measure of a departure of any background map from its standard. The maximum birefringence found on the first map

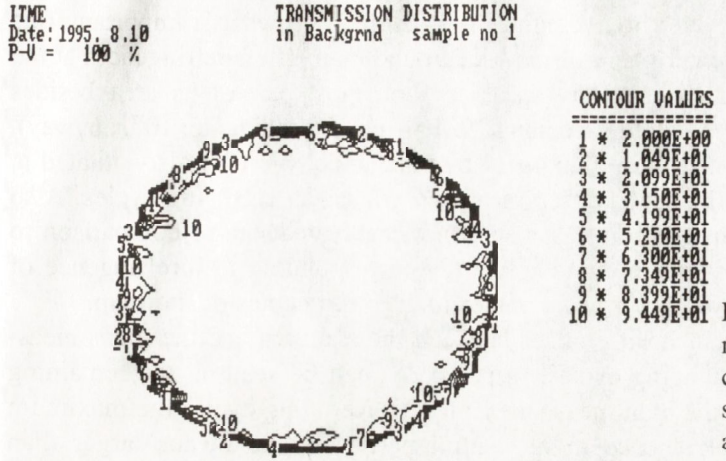

Fig. 9. Background transmission measured with one cycle and corrected for the same measured with 256 averaging cycles.

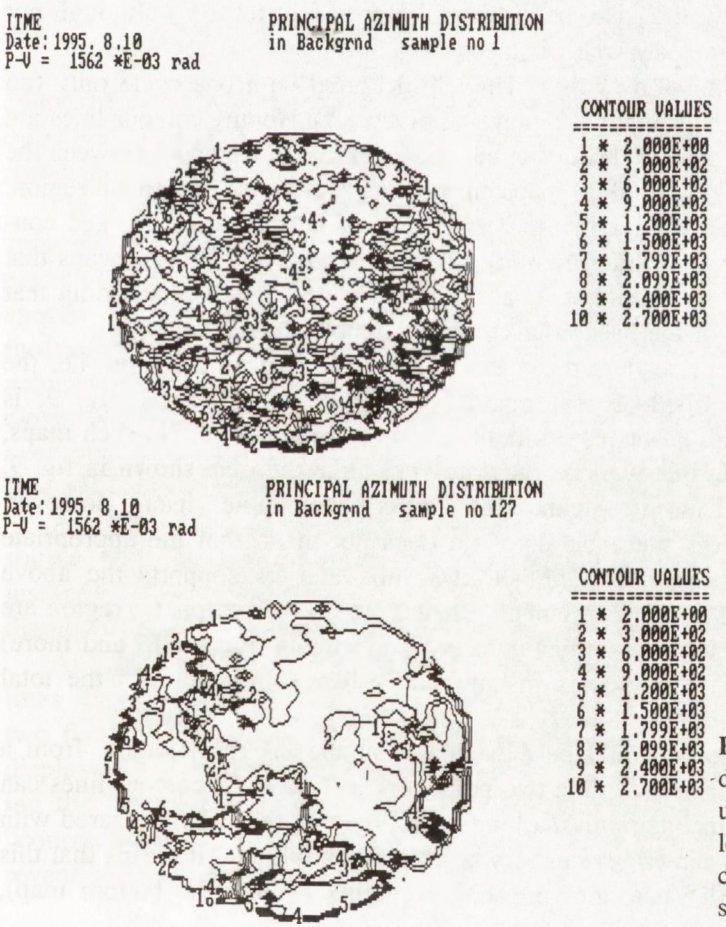

Fig. 10. Principal azimuth distribution of the background measured with one cycle (top map), and with 127 cycles (bottom map), respectively.

measured with only one cycle (no averaging) is $140x10^{-7}$, and what is important, this maximum is situated at the periphery of the background map. The birefringences at the center of the background, or precisely speaking - on most part of its area besides peripheral regions are only slightly exceeding $20x10^{-7}$ (not exceeding $40x10^{-7}$, anyway).

A considerable decrease of the maximum birefringence ($63x10^{-7}$) also situated at the periphery is seen on the second map measured with four averaging cycles. Also the density of the contour lines on this map is noticeably reduced in comparison to the first map. The highest range contour line (2) corresponding to birefringence of $20x10^{-7}$ is more closely to the periphery rather than to the center of the map.

Further reductions of such differences between the standard and the maps measured with 16 and 127 averaging cycles, respectively, can be seen on the remaining two maps. In the case of the map measured with 127 averaging cycles the maximum residual background birefringence in its central part is by no means larger than approximately $2x10^{-7}$ (contour line no. 1). The higher range contour lines (2 and 3), corresponding to birefringences of $20x10^{-7}$ and $40x10^{-7}$, respectively, can be found entirely at the perimeter itself. Also the highest birefringence ($62x10^{-7}$) although not marked on the map is situated at the perimeter.

Figure 9 shows transmission of the "sample" measured with one cycle only (no averaging) in relation to the standard (256 averaging cycles). No any contour lines are seen at the center and on most of the area at all, and any larger differences between the two compared (divided by each other) maps emerge solely from the peripheral region. At the periphery, however, a fall-down to zero transmission (the lowest marked contour lines correspond to a 2 % transmission) can be observed, and it also means that any results of transmission measurements at the periphery of a wafer (providing that the wafer covers all area of the background) can be completely untrue.

The author informs the readers that the width of the peripheral region, i.e. the region which can be defined as that marked by the contour lines in fig. 9, is constantly decreasing with an increased number of averaging cycles. No such maps, however, are presented in this work as they are very alike the map shown in fig. 9, and the only difference being in thickness of the peripheral region itself. However, decreasing thickness of the pheripheral region does not mean that the appropriate transmission loss is also reduced. In fact, it is not, and its supports the above conclussion that transmission measurements carried out on the peripheral region are basically untrue. Fortunately, for larger number of averaging cycles (16 and more) the width of the peripheral region is insignificantly low compared with the total diameter of the map.

As no true birefringence could be expected from the background, i.e. from a relatively thin layer of air between the two polarizers, a "mash" of contour lines can be seen on the top principal azimuth map in fig. 10, the one that was measured with one cycle. Practically all directions in every point are possible and it means that this map is an isotropic-like. When applying 127 averaging cycles (the bottom map),

however, density of the contour lines has greatly decreased and one can even observe a radial-like (but greatly perturbated) principal azimuth distribution. This quasi-radial distribution is a cue for the author, since the air-gap between the two polarizers can not simulate any birefringent pattern at all. The answer to the cue might be plates of the polarizers (the sheet polarizers are glued between two red-filter plastic plates) that can be stressed to some extent by heat absorbed by them from the light beam. This could explain a radial-like symmetry of the principal azimuth distribution.

Before closing this chapter the author would like to return to table 1 where a competition between accuracy and the data acquisition time is marked. Generally speaking that time should be as short as possible, since within a short period of time any larger fluctuations of the light source's power and/or its spectral characteristic (peak wavelength), as well as that of the TV-camera are improbale. Besides, the increased data acquisition time would result in a considerable increase of inspection costs in factories producing large quantities of optical materials. From the results presented in this chapter, however, it can be duly concluded that applying only one cycle (no averaging) is insatisfactory in any circumstances, neither in factory check, nor in scientific research work. From practical point of view the number of averaging cycles should be somewhere between 4 and 16, and the author has chosen 10 averaging cycles as a standard for most investigations of wafers. Therefore, if no other indications are given the subsequent maps presented in this work have been measured using 10 averaging cycles.

On the other hand, however, increasing the data acquisition time from c.a. 43 seconds (10 cycles) to c.a. 448 seconds (127 cycles) can produce fruitful results, especially in scientific research work, when no particular time-schedule or extremal speeds of investigations (check) are required. The author is convinced that the theoretically calculated retardation error/sensitivity of 4×10^{-3} radians (0.2°) can be achieved in practical circumstances only when the number of averaging cycles is close to 100. This can be concluded from the background map measured with 127 averaging cycles (fig. 7), but not from the map measured with either 16 or 32 cycles (not shown in this work).

Anyway, in no circumstances the periphery of the map should be treated as a source of close-to-true results, and the user of the arrangement has to keep it instantly in his mind. A good habit would be also to use (if possible) a larger diameter of the background than of the wafer itself.

At last one more thing has to be mentioned here. This is density of the contour lines that are displayed on a particular map. The density of such lines depends on two factors : the peak value of a measured quantity and a maximum range of the display (MRD) that can be adjusted by the user of the computer's program. Adjusting the MRD either below, or equal to, or above the peak value, it is possible to "contract" or to "elongate" the scale of the displayed contours and thus to better reveal some peculiarities and details of the map.

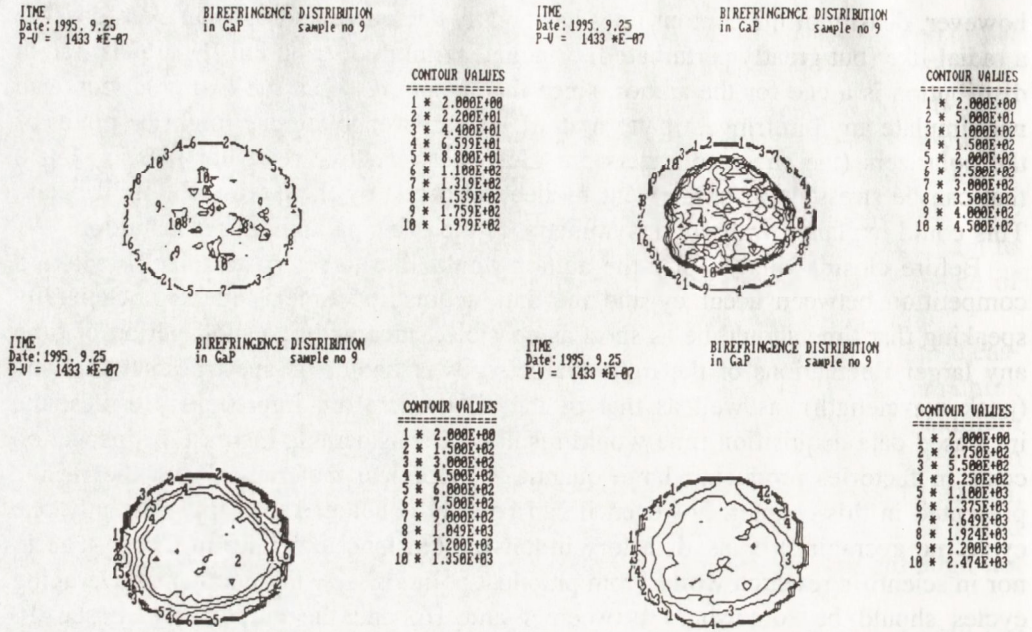

Fig. 11. Residual birefringence distribution measured in <111> oriented, 3.4 mm thick S:doped GaP wafer. The maximum range of the display is 220 ($x10^{-7}$) (top left map), 500 (top right), 1500 (bottom left), and 2750 (bottom right).

This problem is in a certain way also connected with optimization of sensitivity of the measurements, since by adjusting the MRD one can reveal (or not) some of the defects that can appear in the wafer. For example, four maps of the same GaP wafer displayed in different MRD scales are shown in fig. 11. The wafer was cut out perpendicularly to the Czochralski-grown S:doped crystal's axis. The crystal itself exhibited a core-like region at the center. On the first map (top left in fig. 11) a certain perturbance in birefringence distribution can be seen at the

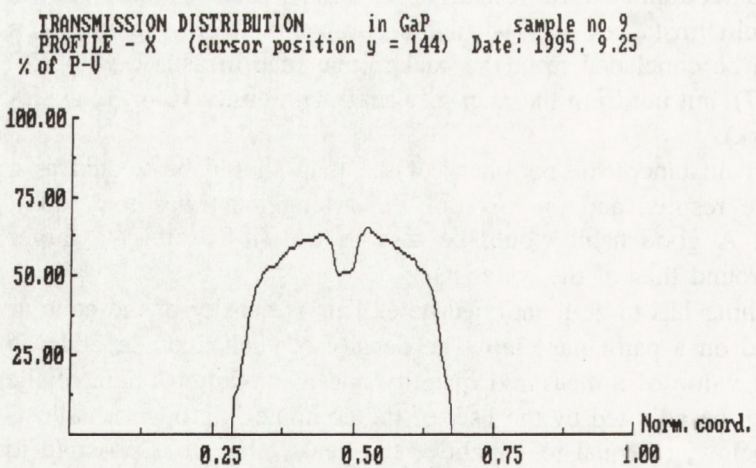

Fig. 12. Transmission distribution horizontal profile in GaP sample,corresponding to fig. 11.

center (also marked on the bottom right map). On the map displayed in the MRD corresponding to the peak value (bottom left map), however, this disturbance is not clearly visible. A clear (quasi)radial residual birefringence distribution is also seen on all maps, especially in the wafer's region close to the perimeter. Depending on the scale this region is also less or more pronounced.

The transmission loss involved by the core region can be also easily observed on the transmission map (a horizontal cross section through the map is shown in fig. 12.). The transmission maps, however, are not frequently displayed nor printed due to their lesser significance compared with the birefringence/stress or the principal azimuth maps.

6. OPTICAL INHOMOGENEITY TESTING IN SEMICONDUCTING AND OXIDE CRYSTALS

In this chapter several birefringence or stress and principal azimuth maps measured in wafers cut out from different parts of semiconducting and oxide crystals are presented together with comments on their optical inhomogeneity having practical implication in material's utilities. However, no transmission maps will be provided here, since in the majority of nowadays-produced materials (usually free from macroscale defects and larger (e.g. stoichiometric) inhomogeneities) transmission through the sample is virtually constant apart of the perimeter effects mentioned in the preceeding chapter. In the case of calculating $LiNbO_3$ stress maps the author has used the data on its refractive indices published by D. Nelson and R. Mikulyak [34] and on its piezooptical coefficients published by E. Spencer, P. Lenzo, and A. Ballman

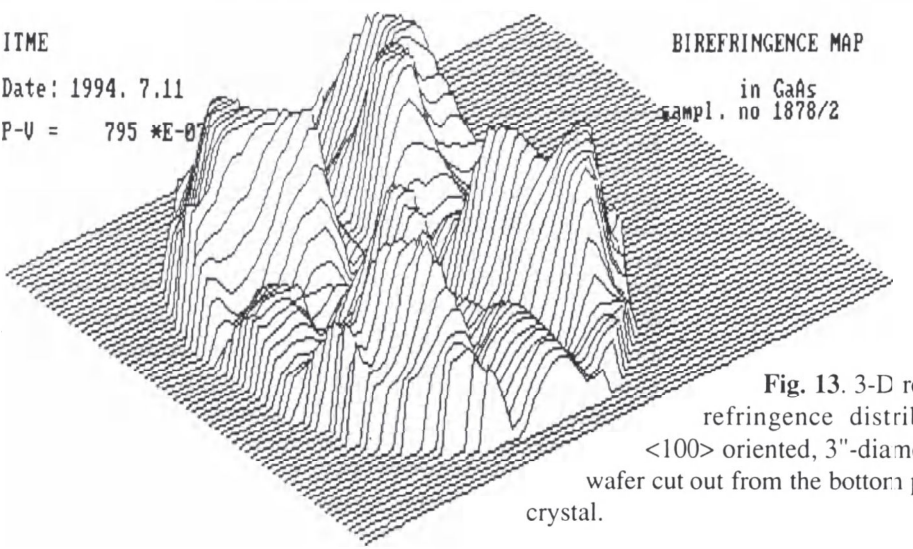

Fig. 13. 3-D residual birefringence distribution in <100> oriented, 3"-diameter GaAs wafer cut out from the bottom part of the crystal.

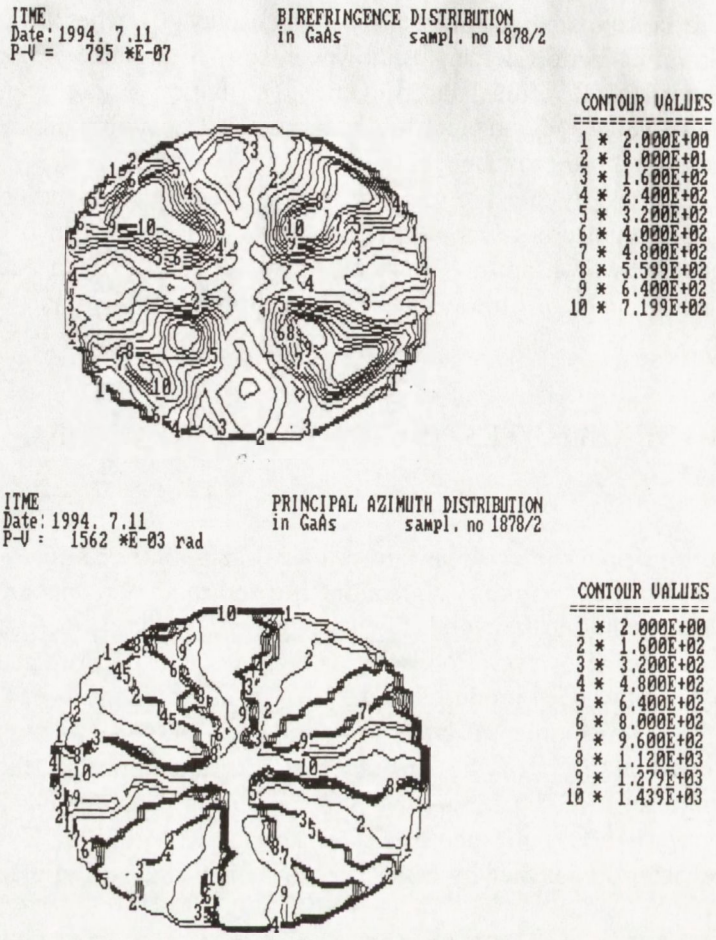

Fig. 14. 2-D residual birefringence (top) and the principal azimuth (bottom) maps of the GaAs wafer, corresponding to fig. 13.

[35].

A three-dimensional (3-D) residual birefringence map in a <100> oriented, 3"-diameter GaAs wafer is shown in fig. 13, whereas the two-dimensional (2-D) birefringence and the principal azimuth maps of this wafer are shown in fig. 14, respectively. The 3-D maps, although very picturesque, are usually much less readable than the adequate 2-D maps, and hence, the latter will be more frequently presented in this work. The four birefringence maxima lying along the <011> directions are a typical case for samples cut out perpendicularly to the <100>-growth direction in cubic crystals pulled by the Czochralski method. A quasi-radial principal azimuth (principal radial stress) direction (fig. 14 - bottom map) is an indication of a certain competition between isotropic conditions in Czochralski growth and anisotropic properties of the crystal pulled in the <100> direction.

A set of two such maps for GaAs wafer cut out from another <100> oriented GaAs crystal is shown in fig. 15. A four-fold residual birefringence distribution is a little better pronounced on these maps than in the preceeding sample, especially on the principal azimuth map. A characteristic feature in both cases are the plateau-like four maxima on the birefringence maps. However, this is not a case met everytime, and, on the contrary, four sharp and close-to-the-perimeter peaks can be seen on a birefringence map of another GaAs wafer (fig. 16).

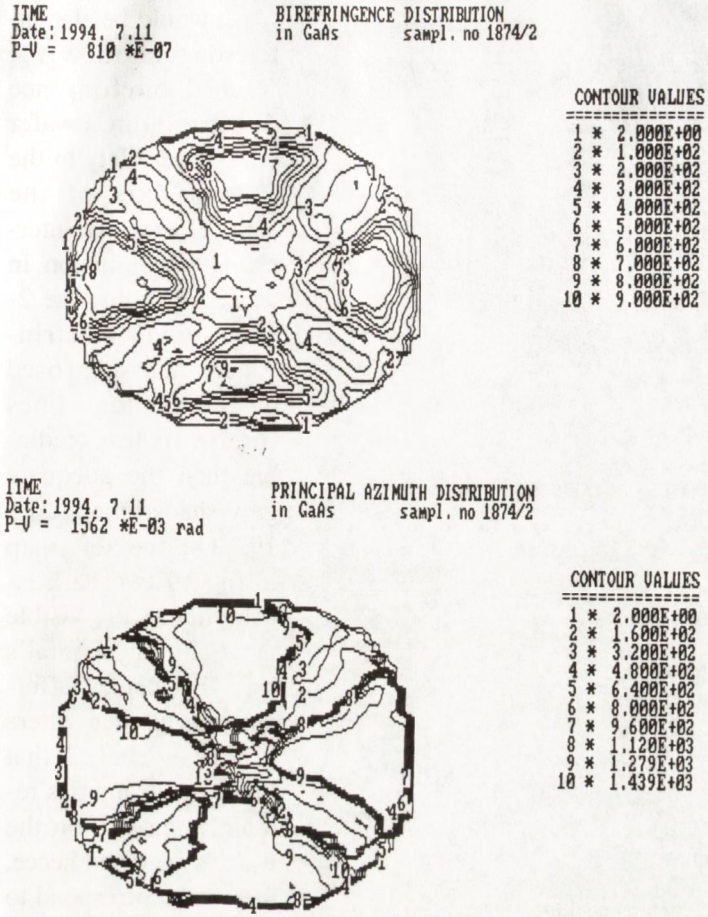

Fig. 15. 2-D residual birefringence (top) and corresponding principal azimuth (bottom) maps of a GaAs wafer cut out from the bottom part of <100> oriented, 3"-diameter GaAs crystal.

Apart from the four-maxima regions found on every birefringence map in <100> oriented GaAs wafers (a typical peak birefringence equals to approximately 8×10^{-5}), the birefringence on the remaining part of the wafers is moderately low and usually does not exceed 2×10^{-5}. The lowest residual birefringences are always found at the center, where they are even equal to zero (as they should be according to theory), and along the <010> directions. The optical inhomogeneity, as defined in chapter 2.1 ranges from zero, through $(1\text{-}2) \times 10^{-5}$ cm^{-1} (in the central parts) up to $(1\text{-}3) \times 10^{-4}$ cm^{-1} in the vicinity of the maxima. Providing that GaAs is used for e.g. electrooptic devices it means that the rectangular prisms should be cut out from the central part of the crystals, and in neither case from any other parts lying along the <011> directions and close to the perimeter.

A much more homogeneous and radial-like residual birefringence distribution can be found in wafers cut out perpendicularly to the <111> growth direction in another semiconducting crystals grown by the Czochralski method. A typical example for such GaP wafer is shown in fig. 11 and the corresponding principal azimuth distribution is presented in fig. 17. From this figure it can be concluded that the maximum residual birefringence (stress) in <111>-grown crystals can be found at the perimeter (as it should be) and that the B on most of the wafer's area does not exceed 1×10^{-5} cm^{-1} (the highest range contour line in the central part of approximately 1" diameter is 4, i.e. it corresponds to birefringence of 240×10^{-7}, and hence $B = 240 \times 10^{-7} / 2.5 < 1 \times 10^{-5}$ cm^{-1}).

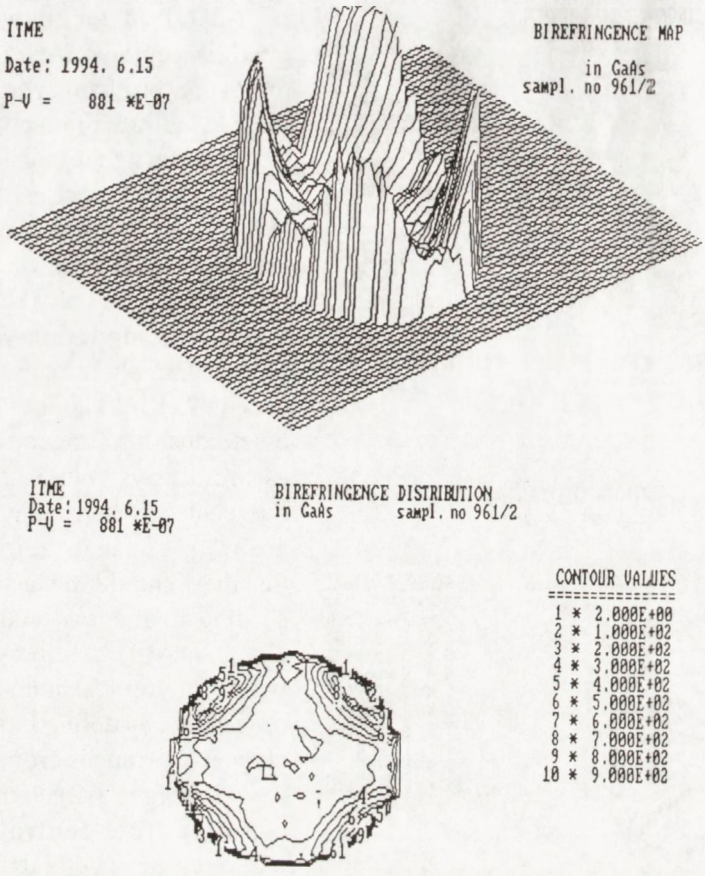

Fig. 16. 3-D (top) and 2-D (bottom) residual birefringence maps of another <100> oriented GaAs wafer cut out from the bottom part of the crystal.

It would be also interesting to show the residual birefringence distribution in a wafer cut out parallely to the growth axis of the same crystal. An interesting phenomenon in this case is that the 2-D residual birefringence map composed of the contour lines (fig. 18) is less readiable than the adequate grey-shaded maps (fig. 19). On the left map in fig. 19 two dark isochromatics are visible parallel to the crystal's axis. By using different interference filters it was evidenced that these isochromatics remain immobile on the wafer's area, and hence, they both correspond to zero-order retardation denoting change in birefringence/stress sign

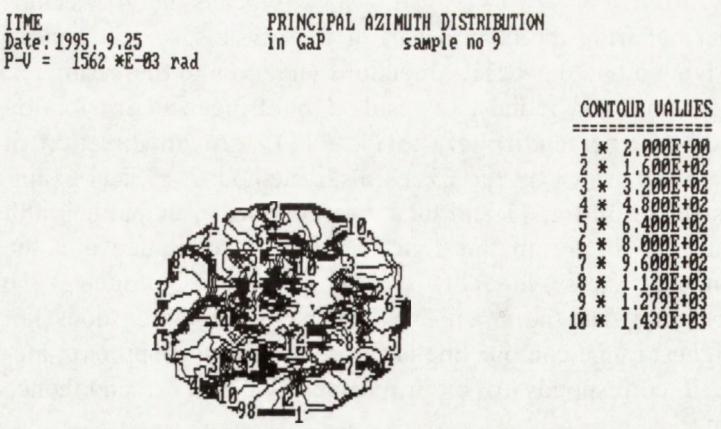

Fig. 17. 2-D principal azimuth map in a 1.5" GaP wafer cut out from the top part of the crystal pulled in the <111> direction, corresponding to fig. 11.

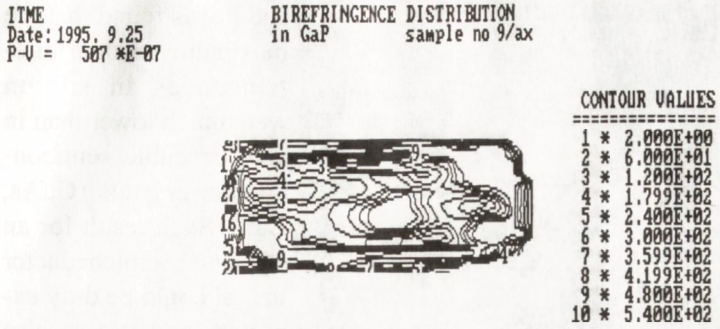

Fig. 18. 2-D residual birefringence map in a wafer (1.5" dia., 2.7" long) cut out parallely to the growth direction of the investigated GaP crystal.

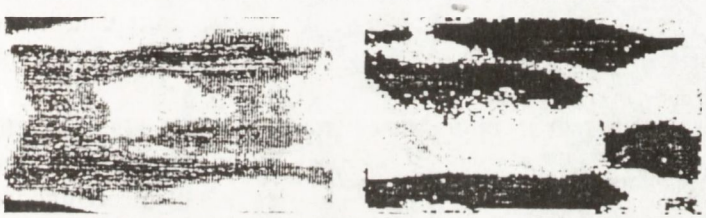

Fig. 19. Grey-shaded maps corresponding to fig. 18, associated with stress-induced birefringence in the investigated GaP wafer. Explanation in the text.

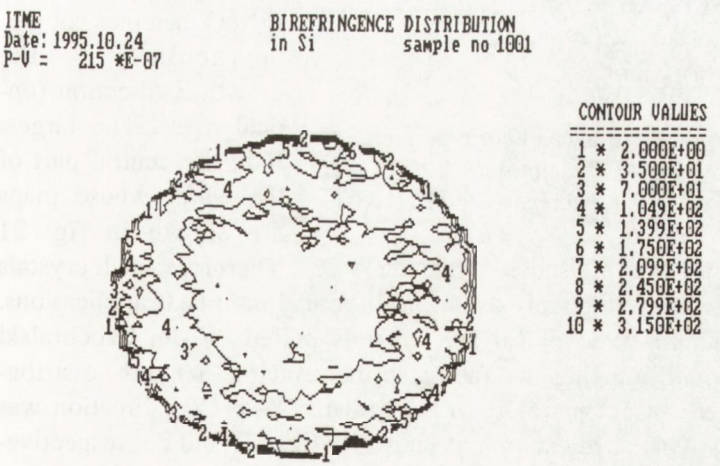

Fig. 20. 2-D residual birefringence map in a 4", 0.36 mm thick wafer cut out from the bottom part of <111> oriented Si crystal.

in the center compared to the two regions close to the perimeter. Such residual birefringence/stress distribution most clearly pronounced in the middle of the crystal and somewhat disturbed in its top (right of the map) and bottom (left of the map) is just expected from theory. The principal azimuth (principal radial residual stress direction) should be constant in such case and perpendicular to the growth direction (the crystal's axis). With certain disturbances discussed above the principal azimuth is, in fact, constant on most of wafer's area (right map in fig. 19) denoted by constant shade areas in both crystal's regions.

A radial or quasi-radial residual birefringence could also be observed in silicon pulled in the <111> direction (fig. 20), and in Z-pulled $LiNbO_3$ (fig. 21). In the case of Si wafers a "white light" corresponding to approximately 1.15 μm wavelength was used,

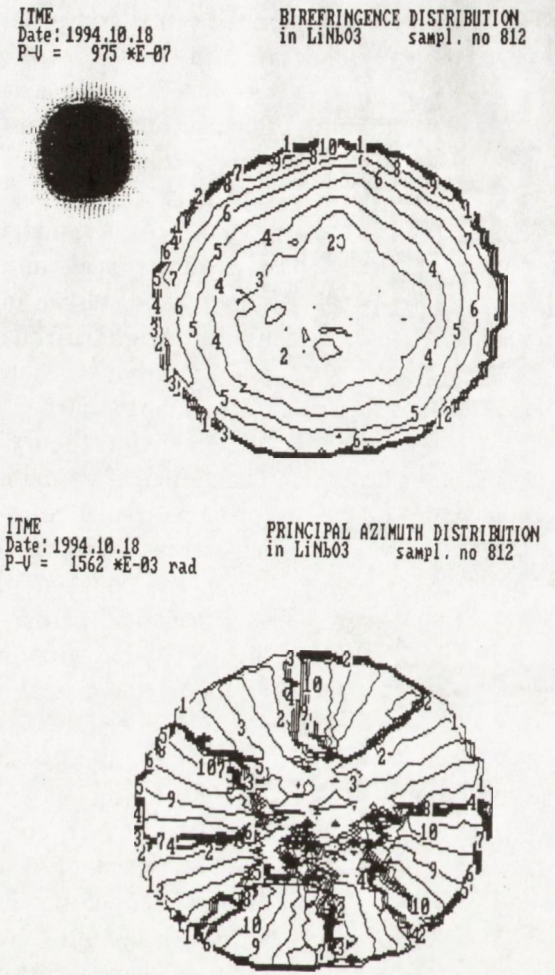

Fig. 21. 2-D residual birefringence (top) and corresponding principal azimuth (bottom) maps of a 4", 0.5 mm thick $LiNbO_3$ wafer cut out from the crystal pulled in the Z-direction (optical axis).

and it was found that the maximum residual birefringences in silicon were much lower than in another cubic semiconducting crystals (GaAs, GaP). Such result for an elemental semiconductor like Si could be duly expected, and it was also found that residual birefringences corresponding to residual stresses were usually much lower in the top parts than in the bottom parts of the crystals.

A clear and practically undisturbed radial residual birefringence distribution evidenced also by the principal azimuth distribution (fig. 21 - bottom map) was a characteristic feature of $LiNbO_3$ samples cut perpendicularly to the growth Z-direction (optical axis). The largest B in the central part of the wafer whose maps are shown in fig. 21 does not exceed 4×10^{-6} cm^{-1} over a distance (diameter) of 2". Therefore, such crystals as that presented above can be effectively used for all optical nonlinear applications.

An interesting feature observed in $LiNbO_3$ crystals pulled by the Czochralski method was that the residual birefringence (and also the principal azimuth) distribution in Z-oriented samples cut out parallely to the growth (Y- or X-) direction was not consistant with theory. One such example is shown in figs. 22 and 23, respectively. A quasi-radial-like birefringence/stress pattern is evidenced from the maps shown in these figures, and they in neither way correspond with the maps for an adequately cut GaP sample shown in figs. 18 and 19. A certain consistency with theory can be

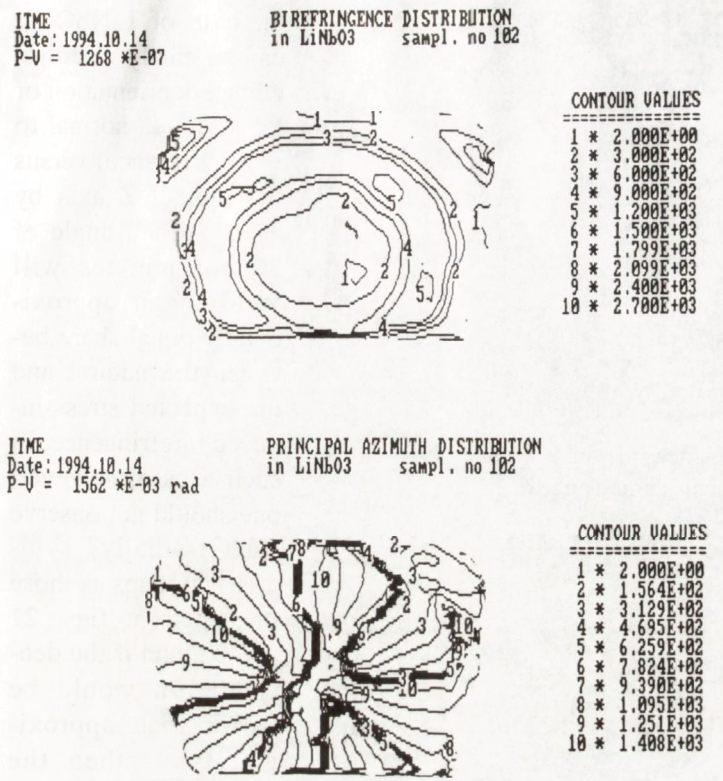

Fig. 22. 2-D residual birefringence (top) and corresponding principal azimuth (bottom) maps of a 3", Z-oriented $LiNbO_3$ wafer cut out from the crystal pulled in the Y-direction.

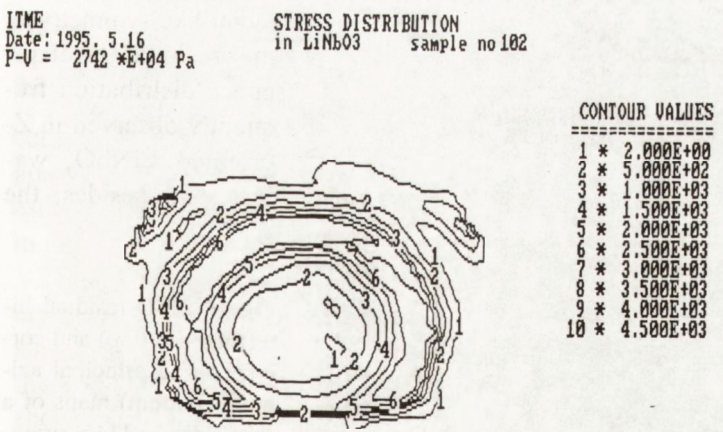

Fig. 23. Residual stress (difference of the principal radial and axial residual stresses, respectively) map of $LiNbO_3$ wafer, corresponding to fig. 22.

observed only in the top part of this $LiNbO_3$ crystal where the birefringence minima between the center and the perimeter can be denoted. Similar results for $LiNbO_3$ crystals were obtained by Sugak et al. [17]. It seems that this discrepancy between theory and measurement is due to several reasons, one of them being an approximately equal width and length of $LiNbO_3$ crystals grown by the Czochralski method (most of the theories are developed for semiinfinite crystals). As is also seen from fig. 22 the central part of the crystal is optically homogeneous ($B < 10^{-5}$ cm^{-1} over a distance exceeding 1.5").

Before closing this part of the chapter on $LiNbO_3$ testing one more thing has to be mentioned here. In the case of highly birefringent crystals like $LiNbO_3$, for example, there is always a certain influence of natural birefringence on the residual birefringence map. For the particu-

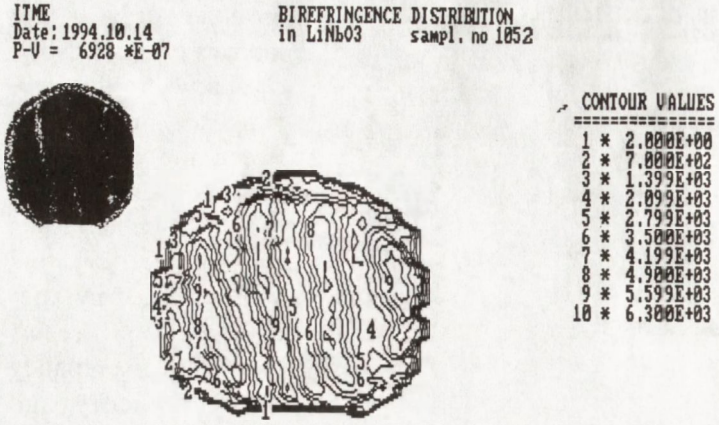

Fig. 24. 2-D natural birefringence map in Y-oriented $LiNbO_3$ wafer showing four distinct isochromatic fringes.

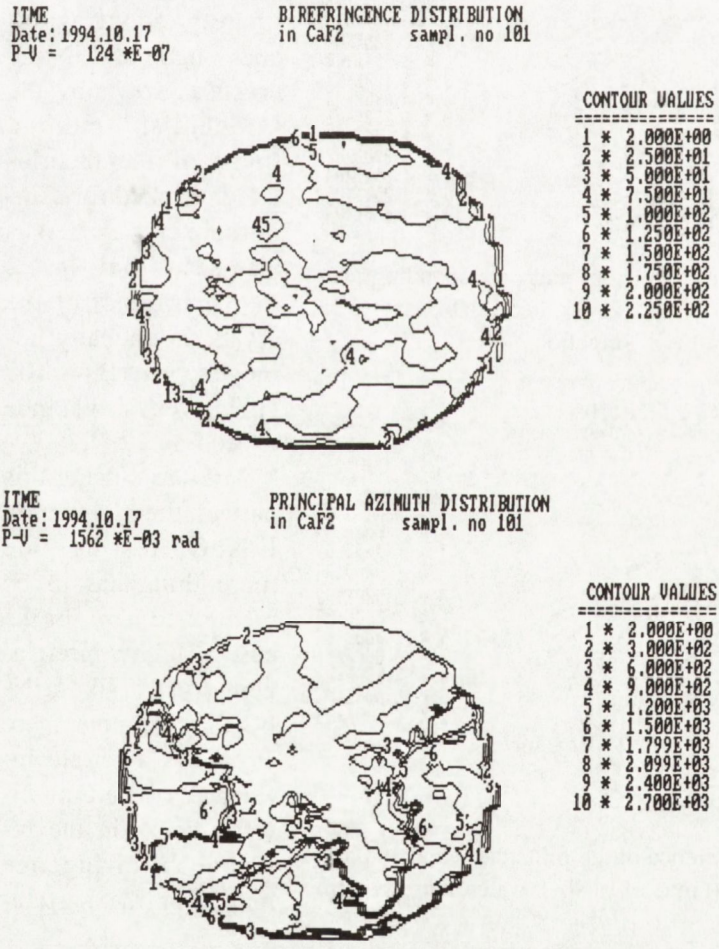

Fig. 25. 2-D residual birefringence (top) and corresponding principal azimuth (bottom) maps of a 3.25" dia., <111> oriented, 6.2 mm thick CaF_2 wafer cut out from the bottom part of the crystal.

lar case of $LiNbO_3$ it can be easily calculated that deorientation of the wafer (a normal to wafer's surface) versus the optical Z axis by even a small angle of 30 arc minutes will yield in an approximately equal share between the natural and the expected stress-induced birefringence. In such a case, however, one should not observe such (radially) symmetrical maps as those presented in figs. 21 and 22, and if the deorientation would be larger than approximately 1° then the maps like that presented in fig. 24 for an Y-oriented $LiNbO_3$ wafer are rather expected. A radial-like symmetry of the residual birefringence distribution frequently observed in Z-oriented $LiNbO_3$ wafers, and besides, the

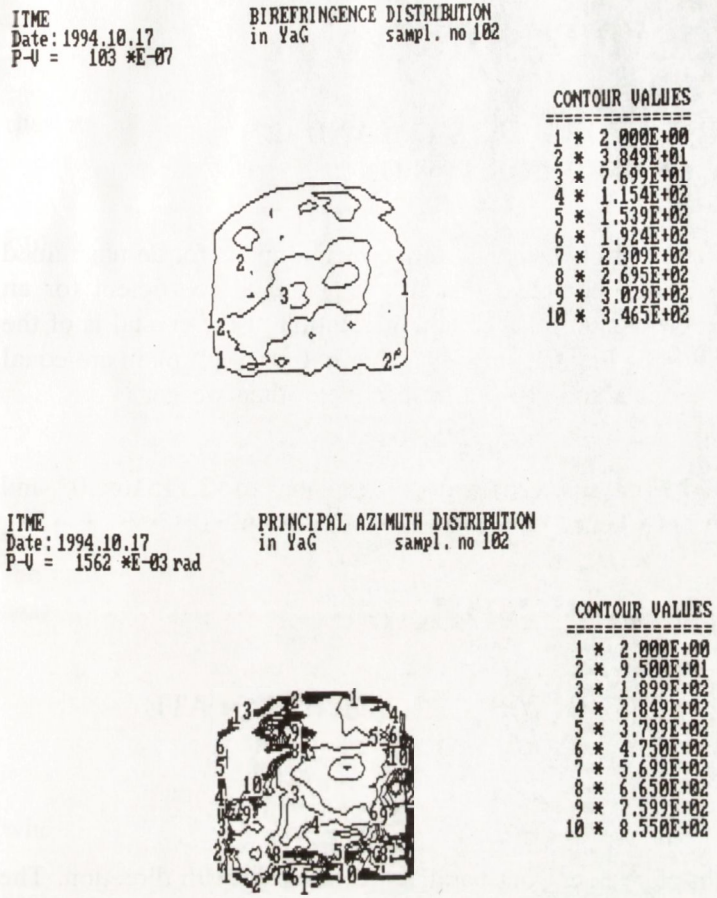

Fig. 26. 2-D residual birefringence (top) and corresponding principal azimuth (bottom) maps of a 1.5" YAG wafer cut out from the top part of the crystal.

dark isoclinic cross rotating on wafer's area when the crossed polarizers are so rotated (fig. 5), indicates that this deorientation is much lower than 30' (usually not exceeding a few minutes). Nevertheless, a certain deorientation always exists, since one is not able to manufacture perfectly Z-oriented samples in the mathematical meaning of this term. If so, the residual birefringence measured by the computer is always larger than its real value in the case of such crystals, and, moreover, this excess can not be fully controlled (or speaking in another words - the error associated with this phenomenon is unknown due to the limited accuracy of the orientation of wafers), since high-precision (seconds) x-ray or optical goniometers are not frequently used in production control. Nevertheless, it can be estimated that this deorientation can be normally kept down to a few minutes resulting in falsification of the residual birefringence by (+) a few percent.

The maximum values of residual birefringences in another oxide, but cubic crystals, like CaF_2 (fig. 25) and $Y_3AL_5O_{12}$ (YAG) (fig. 26) were much lower than the adequate maxima in $LiNbO_3$. The reason is not the size of the crystals (according to theoretical considerations and also to practical experiments the residual stresses should increase with increased diameters of growing crystals), since CaF_2 crystals can be grown as large or even larger than $LiNbO_3$. In the case of YAGs a core region also visible in fig. 26 was a frequently observed phenomenon.

APPENDIX A

DIFFERENCE BETWEEN FORMULAS (26) AND (27) (CHAPTER 3.2) CALCULATED FOR $LiNbO_3$

On the assumption of 871.7 μm wavelength the refractive index for an unstrained crystal n_o=2.2471 [34]. It is next assumed that the piezooptical coefficient (or an adequate combination of coefficients) for a certain orientation of the crystal is of the order of 10^{-12} Pa^{-1} [35]. Providing that the stresses acting in the (x',y') plain are equal and of opposite signs, e.g. 10^7 Pa and -10^7 Pa, respectively, then we get

$n_1=n_o+1/2n_o^3\pi\sigma_{x'}=2.24716$; $n_2=n_o+1/2n_o^3\pi\sigma_{y'}=2.24704$,

and so $\Delta B_{x'}$-$\Delta B_{y'}$ calculated from eqs. (26) and (27) is equal to -2.11516×10^{-5} and -2.11152×10^{-5}, respectively, and hence (2.11516-2.11152)/2.11152=0.17 % .

APPENDIX B

CALCULATION OF $[\Delta B_{(r,t,s)}]$ OR $[\Delta B_{(x',y',z')}]$ (SEE ADEQUATE FORMULAS IN CHAPTER 3.2)

CASE A

Z-oriented $LiNbO_3$ thin plate is cut out parallelly to the Y-growth direction. The axes are as follows: X (horizontal) and Y (vertical) in the (Z) plane. The stresses are acting along X (σ_x - radial component) and Y (σ_y - axial component), respectively. The matrix of the piezooptical coefficients for $LiNbO_3$ in its generalized form for 3 m space group can be acquired e.g. from [6], thus

$$\left[\Delta B_{(x,y,z)}\right]=\begin{bmatrix} \pi_{11} & \pi_{12} & \pi_{13} & \pi_{14} & 0 & 0 \\ \pi_{21} & \pi_{11} & \pi_{13} & -\pi_{14} & 0 & 0 \\ \pi_{31} & \pi_{31} & \pi_{33} & 0 & 0 & 0 \\ \pi_{41} & -\pi_{41} & 0 & \pi_{44} & 0 & 0 \\ 0 & 0 & 0 & 0 & \pi_{44} & -2\pi_{14} \\ 0 & 0 & 0 & 0 & -2\pi_{41} & \pi_{66} \end{bmatrix} \cdot \begin{bmatrix} \sigma_x & 0 & 0 \\ 0 & \sigma_y & 0 \\ 0 & 0 & 0 \end{bmatrix} \qquad \text{(a1)}$$

where $\pi_{66}=2(\pi_{11}-\pi_{12})$. Hence, from multiplication of the above matrices one obtains $\Delta B_x=\pi_{11}\sigma_x+\pi_{12}\sigma_y$, $\Delta B_y=\pi_{21}\sigma_x+\pi_{11}\sigma_y$, and

$$\Delta B_x - \Delta B_y = \pi_{11}(\sigma_x - \sigma_y) - (\pi_{21}\sigma_x - \pi_{12}\sigma_y) \tag{a2}$$

Since matrix $[\pi_{ij}]$ in eq. (a1) is quasi-symmetrical, then a slight approximation that $\pi_{21} \approx \pi_{12}$ can be made, and thus

$$\Delta B_x - \Delta B_y \approx (\pi_{11} - \pi_{12})(\sigma_x - \sigma_y) \tag{a3}$$

From eq. (27) in chapter 3.2 it follows then that

$$\sigma_x - \sigma_y \approx \frac{2\Delta n}{n_o^3(\pi_{11} - \pi_{12})} \tag{a4}$$

CASE B

Z-oriented $LiNbO_3$ thin plate cut out perpendicularly to the Z-growth direction. The axes are as in the preceeding Case A. The stresses are acting along radius (σ_r), making an angle ϕ with the X horizontal axis, and in the direction perpendicular to the radius (σ_t). Since rotation is performed around the Z-axis, hence the rotation matrix [a] (chapter 3.2, eq. (18)) can be used and from eq. (29) one obtains

$$\left[\Delta B_{(r,t,s)}\right] = [a][\pi_{ij}][a^T]\begin{bmatrix}\sigma_r & 0 & 0\\ 0 & \sigma_t & 0\\ 0 & 0 & 0\end{bmatrix} \tag{b1}$$

where $[\pi_{ij}]$ is given in eq. (a1).

When multiplying the 4th rank $[\pi]$ matrices by 2nd rank matrices one has to remember general rules of such multiplication given e.g. in [6]. For example, multiplication of $[\pi_{ij}]$ by $[\sigma_{ij}]$ in the case of ΔB_{22} (in our case $\Delta B_{22}=\Delta B_t$) yields

$$\Delta B_{22} = \pi_{21}\sigma_{11} + \pi_{26}\sigma_{12} + \pi_{25}\sigma_{13} + \pi_{26}\sigma_{21} + \pi_{22}\sigma_{22} + \pi_{24}\sigma_{23} + \pi_{25}\sigma_{31} + \pi_{24}\sigma_{32} + \pi_{23}\sigma_{33}$$

It can be shown that by labourious multiplication of matrices in eq. (b1) one obtains

$$\Delta B_r = (\pi_{11}\sigma_r - \pi_{12}\sigma_t)\cos^2\phi + 2(\pi_{11} - \pi_{12})(\sigma_r - \sigma_t)\sin^2\phi \tag{b2}$$

$$\Delta B_t = -2(\pi_{11} - \pi_{12})(\sigma_r - \sigma_t)\sin^2\phi + (\pi_{21}\sigma_r - \pi_{11}\sigma_t)\cos^2\phi\,. \tag{b3}$$

Hence,

$$\Delta B_r - \Delta B_t = \left[4(\pi_{11} - \pi_{12})\sin^2\phi + \pi_{11}\cos^2\phi\right](\sigma_r - \sigma_t) - (\pi_{21}\sigma_r - \pi_{12}\sigma_t)\cos^2\phi \tag{b4}$$

Again, by making the same approximation as in Case A, i.e. that $\pi_{21} \approx \pi_{12}$, eq. (b4) is, then further simplified

$$\Delta B_r - \Delta B_t \approx (\pi_{11} - \pi_{12})(1 + 3\sin^2\phi)(\sigma_r - \sigma_t) \tag{b5}$$

and hence (chapter 3.2, eq. (27)) it yields

$$\sigma_r - \sigma_t \approx \frac{2\Delta n}{n_o^3(\pi_{11} - \pi_{12})(1 + 3\sin^2\phi)} \qquad (b6)$$

When the map is not plotted in cylindrical coordinates then, of cource, equation (a4) is also valid in such case.

7. REFERENCES

[1] Bajor A.L.: Automated polarimeter-macroscope for optical mapping of birefringence, azimuths, and transmission in large area wafers. 1. Theory of the measurement. Rev. Sci. Instrum., 66, 1995, 4, 2977-2990

[2] Bajor A.L., Kukla M.J., Piątkowski T., Sałbut L., Spik A., Szwedowski A.: ibid. 2. Measurement setup and results. Rev. Sci. Instrum., 66, 1995, 4, 2991-2995

[3] Hauge P.S.: Mueller matrix ellipsometry with imperfect compensators. JOSA, 68, 1978, 11, 1519-1528

[4] Modine F.A., Jellison Jr. G.E., Gruzalski G.R.: Errors in ellipsometry measurements made with a photoelastic modulator. JOSA, 73, 1983, 7, 892-900

[5] Goldstein D.H., Chipman R.A.: Error analysis of a Mueller matrix polarimeter. JOSA, A7, 1990, 4, 693-700

[6] Nye J.F.: Physical properties of crystals. Their representation by tensors and matrices. Oxford 1957, Clarendon Press

[7] Born M., Wolf E.: Principles of optics. 3-rd ed., 1969, Pergamon Press

[8] Bergman J.G., Ashkin A., Ballman A.A., Dziedzic J.M., Levinstein H.J., Smith R.G.: Curie temperature, birefringence, and phase-matching temperature variations in $LiNbO_3$ as a function of melt stoichiometry. Appl. Phys. Lett., 12, 1968, 3, 92-94

[9] Midwinter J.E.: Lithium niobate: effects of composition on the refractive indices and optical second-harmonic generation. JAP, 39, 1968, 7, 3033-3038

[10] Frukacz Z., Kisielewski J., Szydlak J.: YAG:Er^{3+} crystal growth for laser application. Opto-Electronics Rev., 1, 1993, 21-22

[11] Kobayashi N., Iwaki T.: A thermoelastic analysis of the thermal stress produced in a semi-infinite cylindrical single crystal during the Czochralski growth. J. Cryst. Growth, 73, 1985, 96-110

[12] Nash F.R., Boyd G.D., Sargent M. (III) and Bridenbaugh P.M.: Effect of optical inhomogeneities on phase-matching in nonlinear crystals. JAP, 41, 1970, 6, 2564-2576

[13] Tsuya H., Fujino Y., Sugibuchi K.: Dependence of SHG on crystal inhomogereity. JAP, 41, 1970, 6, 2557-2563

[14] Bakhirin Yu. A., Bykovskii Yu. A., Ukraintzev W.A., Tchist'yakov A.A., Yakupov T.M.: Investigation of power soft-tuning in parametric generation of the infrared in highly optically homogeneous $LiNbO_3$ crystals. Kristallografiya, 36, 1991, 5, 1226-1230

[15] Ivanova Z.I., Kovrygin A.I., Lutchinskii G.W., Pashkovitch L.N., Rubinina N.M., Kholodnyh A.I.: Manufacturing and optical inhomogeneity investigation of 45° $LiNbO_3$ crystals used for parametric optical generators. Kvant. Elektron., 7, 1980, 1013

[16] Shen Y.R.: The principles of nonlinear optics. 1984, John Willey & Sons, Inc.

[17] Sugak D.Yu., Matkovskii A.O., Korobenko E.A., Mikhalevich A.T., Solskii I.M., Gaba V.M., Kopko B.N.: Optical Elements for near infrared spectra region from high optical quality lithium niobate single crystals. Proc. SPIE, 2206,1995

[18] Petrova D., Pavloff O., Marinov P.: Optical quality and laser characteristics of YAG:Nd crystals grown by the Bridgman-Stockbarger method. J. Cr. Growth, 99, 1990, 841-844

[19] Pracka I., Giersz W., Świrkowicz M., Pajączkowska A., Kaczmarek S., Mierczyk Z.: The Czochralski growth of $SrLaGa_3O_7$ single crystals and their optical and lasing properties. Mater. Sci. Eng., B26, 1994, 201-206

[20] Frukacz Z., Kisielewski J., Mierczyk Z., Żendzian W.: Growth of Cr,Tm,Ho:YAG crystal and its optical and laser characteristics", Proc. SPIE, 2202, 1995, 164-170

[21] Kotake H., Takasu Shin: Quantitative measurement of stress in silicon by photoelasticity and its application. J. Electrochem. Soc., 127, 1980, 1, 179-184

[22] Jungbluth E.D., Chiao H.C.: Intense interjunction strain in phosphorus-diffused silicon. J. Electrochem. Soc., 115, 1968, 4, 429-433

[23] Lederhandler S.R.: Infrared studies of birefringence in silicon. JAP, 30, 1959, 11, 1631-1638

[24] Honstra J., Penning P.: Birefringence due to residual stress in silicon. Philips Res. Repts., 14, 1959, 237-249

[25] Pluta M.: Polarized-light microinterferometry. WNT 1991, in Polish

[26] Ratajczyk F.: Optics of anisotropic media. PWN 1994, in Polish

[27] Bond W.L.: Measurement of refractive indices of several crystals. JAP, 36, 1965, 5, 1674-1677

[28] Becker H., Brach D., Otto A., Weber H.-J.: Sensitive and selective polarimeter for application in crystal optics. Rev. Sci. Instrum., 62, 1991, 1196-1205

[29] Hayden J.E., Jacobs S.D.: Automated spatially scanning ellipsometer for retardation measurements of transparent materials. Appl. Opt., 32, 1993, 6256-6263

[30] Yamada M.: High sensitivity computer-controlled infrared polariscope. Rev. Sci. Instrum., 64, 1993, 1815-1821

[31] Kitamura K., Kimura S., Miyazawa Y., Mori Y., Kamada O.: Stress-birefringence associated with facets of rare-earth garnets grown from the melt; a model and measurement of stress-birefringence observed in thin sections. J. Cryst. Growth. 62, 1983, 351-359

[32] Indenbom V.L., Osvensky V.B.: Theoretical and experimental studies of generation of stress and dislocations in growing crystals. Growth of Crystals, 13, 1986, 279-290

[33] Koechner W., Rice D.K.: Effect of birefringence on the performance of linearly polarized YAG:Nd lasers. IEEE J. Quant. Electron., QE-6, 1970, 9, 557-566

[34] Nelson D.F., Mikulyak R.M.: Refractive indices of congruently melting lithium niobate. JAP, 45, 1974, 12, 8, 3688-3689

[35] Spencer E.G., Lenzo P.V., Ballman A.A.: Dielectric materials for electrooptic, elastooptic, and ultrasonic device applications. Proc. IEEE, 55, 1967, 2074-2108

ACKNOWLEDGMENT

The author is greatly indebted to Professor Maksymilian **Pluta** from the Institute of Applied Optics (Warsaw) for reviewing of this text and many helpful comments and suggestions.

NIEKTÓRE PROBLEMY BADAŃ NIEJEDNORODNOŚCI OPTYCZNEJ KRYSZTAŁÓW ZA POMOCĄ POLARYMETRU OBRAZOWEGO

Streszczenie

W pracy przedstawiono pokrótce główne problemy związane z badaniem niejednorodności optycznej materiałów (głównie kryształów), takie jak: źródła tej niejednorodności i jej wpływ na własności aplikacyjne materiału, wady i zalety różnych metod badawczych, w tym zautomatyzowanych metod polarymetrii obrazowej. Przedstawiono zasady działania i własności użytkowe skonstruowanego w ITME polarymetru obrazowego, umożliwiającego badanie płaskorównoległych próbek materiałów o średnicy do 150 mm i grubości do 10 mm, w zakresie długości fal promieniowania elektromagnetycznego 0.4 - 1.15 μm. Polarymetr umożliwia wyznaczenie różnych wielkości fizycznych z następującymi dokładnościami: dwójłomność $\leq 5x10^{-7}$, główny azymut (kierunek jednego z naprężeń głównych) < 1°, transmisji < 1 % . Działanie przyrządu zilustrowano licznymi wynikami badań, zwłaszcza materiałów półprzewodnikowych i elektrooptycznych wytwarzanych w ITME, takich jak GaAs i $LiNbO_3$.

НЕКОТОРЫЕ ПРОБЛЕМЫ ИССЛЕДОВАНИЯ ОПТИЧЕСКОЙ НЕОДНОРОДНОСТИ КРИСТАЛЛОВ МЕТОДОМ ПОЛЯРИМЕТРИИ ИЗОБРАЖЕНИЙ

Краткое содержание

В работе представлены: принцип действия, конструкция и эксплутационные данные линейного полярископа, используемого для исследования оптической неоднородности (вызываемой в частности остаточными напряжениями) в пластинках кристаллических материалов. Основные данные прибора: диапазон длин волн 0.4-1.15 мкм (CCD телевизионная кремниевая камера); размеры пластинок - диаметер до 150 мм, толщина до 10 мм; ошибки измерений - двойное лучепреломление $\leq 5x10^{-7}$, главный азимут < 1°, оптическое пропускание < 1%. Представлены примеры использования прибора (кроме трёх вышеуказанных величин может быть построена карта остаточных напряжений по разнице главных напряжений) для исследования оптической неоднородности в полупроводниковых и кислородсодержащих кристаллах, полученных в ИТЭМ, таких как GaAs и $LiNbO_3$.

Druk: Zakład Poligraficzny J. Dymczak, S. Prasek, Piastów, ul. Mazurska 9